Elsevier Editorial System(tm) for Remote Sensing of Environment
Manuscript Draft

Manuscript Number:

Title: Parameterization of an ecosystem light-use-efficiency model for predicting savanna GPP using MODIS EVI

Article Type: Original Research Paper

Keywords: Savanna, GPP, MODIS, EVI, eLUE, NATT, OzFLUX

Corresponding Author: Dr. Alfredo R. Huete, PhD

Corresponding Author's Institution: University of Technology Sydney

First Author: Xuanlong Ma

Order of Authors: Xuanlong Ma; Alfredo Huete, Ph.D.; Qiang Yu, Ph.D.; Natalia Restrepo-Coupe, Ph.D.; Jason Beringer, Ph.D.; Lindsay Hutley, Ph.D.; Kasturi Devi Kanniah, Ph.D.; James Cleverly, Ph.D.; Derek Eamus, Ph.D.

Dear Editor:

Please find attached a manuscript entitled "Parameterization of an ecosystem light-use-efficiency model for predicting savanna GPP using MODIS EVI" for consideration of publication as an original research paper in Remote Sensing of Environment. I declare here that the manuscript has not been submitted and is not being considered for submission to any other journal and that I have no conflict of interest.

I believe this manuscript will be of general interest to the readers of Remote Sensing of Environment. Accurate estimation of carbon fluxes across space and time is of great importance for quantifying global carbon balances. In this study, we proposed a new and improved framework for up-scaling savanna gross primary production (GPP) from eddy covariance (EC) flux tower GPP measures to regional scale utilizing remote sensing without dependency on ground meteorology.

We first assessed seasonal patterns of MODIS vegetation products with seasonal EC tower GPP along an ecological rainfall gradient (the Northern Australian Tropical Transect, NATT) encompassing tropical wet to dry savannas. The EVI showed the strongest local site and cross-site relationships with tower GPP. The EVI relationship with tower GPP was further strengthened through coupling with ecosystem light-use-efficiency (eLUE), defined as the ratio of GPP and Photosynthetically Active Radiation (PAR). Two savanna landscape eLUE models, driven by top-of-canopy incident PAR or top-of-atmosphere incident PAR were then parameterized. GPP predicted using the eLUE models agreed well with tower GPP and were considerably improved relative to the MOD17 GPP product.

As such, this manuscript should fit well in the areas of terrestrial sensing, biophysical parameters retrieval, ecology, and environmental science. This manuscript has been prepared to comply with Remote Sensing of Environment's formatting guide. The manuscript includes 4 tables and 10 figures. The total length, not including references, is ca. 9300 words.

I look forward to hearing from you.

Kind regards,

Xuanlong Ma

- We assessed five MODIS vegetation products for tracking seasonal tower GPP over Australian savannas;
- EVI was a strong measure of ecosystem light-use-efficiency (eLUE) defined as GPP/PAR;
- EVI parameterized eLUE models driven by PAR predicted tower GPP with good accuracy;
- eLUE models reduced green-up and brown-down phenophase impacts on satellite *versus* tower GPP relationships.

Parameterization of an ecosystem light-use-efficiency model for predicting savanna GPP using MODIS EVI

Xuanlong Ma [a,b,c], Alfredo Huete [b,*], Qiang Yu [b], Natalia Restrepo-Coupe [b], Jason Beringer [d], Lindsay B. Hutley [e], Kasturi Devi Kanniah [f], James Cleverly [b,g], Derek Eamus [b,g,h]

[a] Key Laboratory of Water Cycle and Related Land Surface Processes, Institute of Geographic Sciences and Natural Resources Research, Chinese Academy of Sciences, Beijing, China, 100101;

[b] Plant Functional Biology and Climate Change Cluster (C3), University of Technology, Sydney, NSW, Australia, 2007;

[c] University of Chinese Academy of Sciences, Beijing, China, 100049;

[d] School of Geography and Environmental Science, Monash University, Melbourne, Victoria, Australia, 3800;

[e] Research Institute for the Environment and Livelihoods, Charles Darwin University, Casuarina, Northern Territory, Australia, 0909;

[f] Department of Geoinformation, Faculty of Geoinformation and Real Estate, Universiti Teknologi Malaysia, Skudai, Johor, Malaysia, 81310;

[g] Australian Supersite Network, Terrestrial Ecosystem Research Network, University of Technology, Sydney, NSW, Australia, 2007;

[h] National Centre for Groundwater Research and Training, University of Technology, Sydney, NSW, Australia, 2007

* Corresponding author *at: Plant Functional Biology and Climate Change Cluster, University of Technology, Sydney, Broadway, NSW, 2007, Australia.* alfredo.huete@uts.edu.au, *+61 2 9514 4084*

Abstract

Accurate estimation of carbon fluxes across space and time is of great importance for quantifying global carbon balances. Current production efficiency models for calculation of gross primary production (GPP) depend on estimates of light-use-efficiency (LUE) obtained from look-up tables based on biome type and coarse-resolution meteorological inputs that can introduce uncertainties. Plant function is especially difficult to parameterize in the savanna biome due to the presence of varying mixture of multiple plant functional types (PFTs) with distinct phenologies and responses to environmental factors. The objective of this study was to find a simple, robust method to up-scale savanna GPP from local, eddy covariance (EC) flux tower GPP measures to regional scales utilizing remote sensing. Here we assessed seasonal patterns of Moderate Resolution Imaging Spectroradiometer (MODIS) vegetation products with seasonal EC tower GPP (GPP_{EC}) at 4 sites along an ecological rainfall gradient (the Northern Australian Tropical Transect, NATT) encompassing tropical wet to dry savannas.

The enhanced vegetation index (EVI) showed the strongest local site and cross-site (R^2 = 0.84) relationships with GPP_{EC}. The EVI relationship with GPP_{EC} was further strengthened though coupling with ecosystem light-use-efficiency (eLUE), defined as the ratio of GPP and Photosynthetically Active Radiation (PAR). Two savanna landscape eLUE models, driven by top-of-canopy incident PAR (PAR_{TOC}) or top-of-atmosphere incident PAR (PAR_{TOA}) were then parameterized. GPP predicted using the eLUE models agreed well with GPP_{EC}, with R^2 of 0.85 (RMSE = 0.76 g C m^{-2} d^{-1}) and 0.88 (RMSE = 0.70 g C m^{-2} d^{-1}) for PAR_{TOC} and

PAR_{TOA}, respectively, which were considerably improved to the MOD17 GPP product (R^2 = 0.58, RMSE = 1.43 g C m^{-2} d^{-1}). The eLUE model also normalized seasonal green-up and brown-down hysteresis effects between GPP_{EC} and MODIS satellite products. The consistent estimation of GPP across phenophases suggests that the eLUE model effectively integrates variations in photosynthetic capacity and environmental stress on photosynthesis. These results demonstrate that region-wide savanna GPP can be estimated fairly accurately using remote sensing without dependency on ground meteorology.

Keywords:

Savanna, GPP, MODIS, EVI, eLUE, NATT, OzFLUX

1 Introduction

Measurement of landscape carbon fluxes is essential in global change studies (Baldocchi et al., 2001), but remain a challenge to measure in the field, resulting in a scarcity of measurements available to validate and assess uncertainties in models and satellite products. By observing broad-scale patterns of ecosystem functioning, remote sensing can complement the restricted coverage afforded by eddy covariance (EC) tower flux measures of gross primary production (GPP). Remote sensing estimates of GPP primarily utilize two technical approaches: (1) process models based on the light-use-efficiency (LUE) concept (Running et al., 2004; Xiao et al., 2005), and (2) empirical models based on relationships between flux tower estimates of GPP and satellite spectral vegetation indices (VIs) (Rahman et al., 2005; Gitelson et al., 2006; Huete et al., 2006; Sims et al., 2008).

The LUE concept was first proposed by Monteith (1972) to estimate GPP by defining the amount of carbon fixed through photosynthesis as proportional to the solar energy absorbed by the plant. LUE, the energy conversion coefficient, can either be defined as the ratio of

GPP to incident photosynthetic active radiation (PAR) or absorbed photosynthetic active radiation (APAR) (Gower et al., 1999), with APAR as the product of PAR and the fraction of absorbed photosynthetically-active radiation (fAPAR) (Monteith, 1972; Running et al., 2004). LUE models defined from APAR have been widely adopted to estimate GPP globally with the use of fAPAR and LUE (ε) (Monteith, 1972):

$$\mathrm{GPP} = \varepsilon \times \mathrm{fAPAR} \times \mathrm{PAR} \tag{1}$$

The MODIS GPP product (MOD17) is based on the LUE concept and provides the first operational and near-real-time calculation of global GPP (Running et al., 2004; Zhao et al., 2005). The MOD17 algorithm for calculating daily GPP is expressed as (Running et al., 2004):

$$\mathrm{GPP} = \varepsilon_{\mathrm{max}} \times 0.45 \times \mathrm{SW}_{\mathrm{rad}} \times \mathrm{fAPAR} \times f(\mathrm{VPD}) \times f(\mathrm{T}_{\mathrm{min}}) \tag{2}$$

where ε_{max} is the maximum light-use-efficiency, which is biome specific and obtained from a look-up table; SW_{rad} is short-wave downward solar radiation, of which 45% is assumed to be PAR; f(VPD) and $f(T_{min})$ are the reduction scalars for water stress and low temperature respectively (Running et al., 2004).

A major limitation of current LUE-based production efficiency models is that there are no direct measurements of LUE available at landscape scales. LUE is very difficult to parameterize since it varies significantly among vegetation type (Turner, 2003; Kergoat et al., 2008), across seasons and phenophases (Sims et al., 2006; Jenkins et al., 2007), and under different types of environmental stress (Ruimy et al., 1995). Consequently, maximum LUE values have to be specified for a limited number of biome types and then down-regulated by environmental stress scalars derived from coarse resolution, interpolated meteorological inputs (Zhao et al., 2005; Heinsch et al., 2006), which contribute uncertainties in output GPP

(Heinsch et al., 2006; Yuan et al., 2010; Sjöström et al., 2013). Some studies reported that LUE models, when properly parameterized with site-level meteorological measurements, can provide good estimates of flux tower derived GPP (Turner et al., 2003; Kanniah et al., 2009), while other studies found only moderate improvements (Sjöström et al., 2013).

The MODIS GPP product has limited accuracy in estimating GPP of savannas (Kanniah et al., 2009; Sjöström et al., 2013; Jin et al., 2013), which are defined as woodland communities with a conspicuous perennial or annual graminoid substrata, with varying proportions of trees, shrubs and graminoids that form a structural continuum (Walker & Gillison, 1982). Across African savanna flux tower site, Sjöström et al. (2013) reported MODIS GPP to underestimate tower-GPP over dry sites in the Sahel region due to uncertainties in the meteorological drivers and fAPAR data and underestimation of ε_{max}. At a woodland savanna site in Botswana, Jin et al. (2013) reported the MODIS GPP product to be substantially lower than tower-GPP during the green-up phase and higher than tower-GPP during the brown-down phase.

Kanniah et al. (2009) confirmed the usefulness of the MODIS GPP product for studying carbon dynamics at a northern Australian savanna site, yet important limitations were found due to the lack of representation of soil moisture in the MODIS GPP algorithm. These suggest a need to consider the limitations of current LUE based methodologies to estimate savanna GPP. Although it may be possible to improve the MODIS GPP product across global savannas by incorporation of a soil moisture term and using better quality meteorological data, it is also worthwhile to consider alternative methods for accurate and consistent remote sensing estimation of global GPP without dependency on numerous inputs (Sims et al., 2008).

Glenn et al. (2008) suggested that remote sensing is more suitable as a scaling tool when ground data are available, rather than for solving complicated physical models. Remote sensing can greatly simplify the up-scaling of ecosystem processes, such as photosynthesis and evapotranspiration, from an expansive network of flux towers to larger landscape units and to regional scales (Glenn et al., 2008). As top-of-canopy measurements, flux towers do not require knowledge of LAI or details of canopy architecture to estimate fluxes (Baldocchi et al., 2001; Glenn et al., 2008). Meanwhile, the measurement footprint of flux towers partially overlaps the pixel size of daily-return satellites (e.g., 250 m for MODIS). With the fast evolving regional and global flux networks (e.g., FLUXNET, AmeriFLUX, AsiaFlux, and OzFLUX) and ongoing space-borne sensors (e.g., Landsat, MODIS and MERIS), enormous opportunities now exist to develop more robust and consistent methods for scaling of carbon fluxes across space and time through better coupling of these two independent sources of observations (Huete et al., 2008).

The spatial extension of tower measured carbon fluxes using satellite spectral VIs have been investigated across a wide range of natural and agricultural ecosystems. For example, Wylie et al. (2003) reported a strong relationship between NDVI and daytime CO_2 flux in a sagebrush-steppe. Over North America, Rahman et al. (2005) found that EVI can provide reasonably accurate estimates of GPP. Sims et al. (2006) further concluded EVI relationships with tower-GPP to be better than that with MOD17 GPP when data from winter periods of inactive photosynthesis were excluded. In Amazonia, Huete et al. (2006) observed a consistent linear relationship between MODIS EVI and tower GPP in both primary forest and converted pasture with MODIS EVI not saturating over the high foliage densities of tropical rainforests. Huete et al. (2008) further extended this study to three distinct Monsoon Asia tropical forest sites and found similar linear relationships between EVI and tower GPP, potentially offering opportunities for region-wide scaling of carbon fluxes across the heterogeneous canopies of Southeast Asia. Over Scandinavian forest sites, Olofsson et al. (2008) reported strong correlations between EVI and GPP, while NDVI exhibited saturation in areas with high foliage density. Across African savannas, Sjöström et al. (2011) found EVI to track the seasonal dynamics of tower GPP more closely than MOD17 GPP. More recently, Ma et al. (2013) observed good convergence between MODIS EVI and tower GPP across northern Australian mesic and xeric savannas, confirming the potential to link these two data sources for estimation of savanna GPP.

Other studies have investigated coupling EVI with satellite retrieved land surface variables for improved predictions of tower derived GPP. For example, Sims et al. (2008) used a Temperature and Greenness (T-G) model, based on EVI and land surface temperature (LST), and substantially improved the correlation between predicted and tower derived GPP across North America compared with MOD17 GPP or EVI alone. Gitelson et al. (2006) found that a Greenness and Radiation (G-R) model, coupling canopy chlorophyll content with PAR, provided a more robust estimation of crop GPP. Peng et al. (2013) applied the G-R model to estimate GPP using chlorophyll-related VIs (VI_{chl}), such as NDVI, EVI, and the wide dynamic range vegetation index (WDRVI), and found high accuracies in GPP estimations over irrigated and rain fed croplands. Wu et al. (2009) also found a tight relationship between canopy total chlorophyll content and GPP/PAR, thereby providing new ways to estimate GPP from chlorophyll-related spectral indices.

From a resource use efficiency perspective, the coupling of VI_{chl} and PAR for the estimation of GPP implies that VI_{chl} is essentially a measure of LUE defined and based on PAR. To distinguish the LUE (ε) based on APAR from LUE based on PAR, we define the former as ε (i.e., GPP/APAR) and the latter as ecosystem light-use-efficiency (eLUE). eLUE can be computed and modelled as:

$$\mathrm{eLUE} = \frac{\mathrm{GPP}}{\mathrm{PAR}} = \mathrm{fAPAR} \times \varepsilon = f(\mathrm{VI_{chl}}) \quad (3)$$

where $f(\mathrm{VI_{chl}})$ can be calibrated by regression with flux tower derived eLUE against $\mathrm{VI_{chl}}$. eLUE (GPP/PAR) differs from ε (GPP/APAR) in that it combines the biological drivers of photosynthesis (fAPAR) with net photosynthetic efficiency (ε) resulting from environmental stress and leaf age phenology. The benefit of using eLUE in up-scaling of GPP is that eLUE does not require partitioning of plant functioning into both fAPAR and ε terms, thus simplifying remote sensing based productivity estimates and reducing associated scaling uncertainties introduced by coarse resolution meteorological inputs and from the need to define biome specific ε_{max} values in mixed tree-grass savannas.

The objectives of this study were to (1) assess seasonal synchronies and performances of various satellite vegetation products and models for tracking seasonal variations in $\mathrm{GPP_{EC}}$ along an ecological rainfall gradient encompassing northern Australia mesic to xeric savannas; (2) to examine the use of ecosystem light-use-efficiency (eLUE) models for up-scaling tower derived GPP to regional scales from purely remote sensing observations without dependency on ground meteorology; and (3) to assess scale issues for extrapolating tower GPP across biologic phenophases, including green-up and brown-down periods.

2 Methods

2.1 Study area

This study focused on a sub-continental scale ecological rainfall gradient of more than 1100 km, which is known as the North Australian Tropical Transect (NATT) (Koch et al., 1995) (Fig. 1). The NATT was conceptualized in the mid-1990s as part of the International Geosphere Biosphere Programme (IGBP) (Koch et al., 1995), together with the Kalahari transect in southern Africa and the SALT (Savanne à Long Terme) transect in West Africa, these three transects have been used extensively in the study of global savannas (Walker et al., 1999).

Carbon flux measurements from four EC flux towers sites located along the NATT transect were used (Fig. 1 & Table 1), including three Eucalypt woodland sites: Howard Springs, Adelaide Rivers, and Daly River (Beringer et al., 2011) and an *Acacia* woodland site: Ti Tree (Eamus et al., 2013; Cleverly et al., 2013). These sites are part of OzFLUX (Australian and New Zealand Flux Research and Monitoring) under the TERN (Australian Terrestrial Ecosystem Research Network). These sites represent the two most common savanna classes present in Australia, namely, *Eucalyptus* (and closely-related *Corymbia*) woodland and *Acacia* woodland.

2.2 Eddy covariance tower derived GPP (GPP_{EC})

The original Level 3 OzFLUX data were pre-processed to ensure consistency among sites and reduce the uncertainties in computed fluxes, including general quality control assessment, removal of outliers, and correction for low turbulence periods. A second-order Fourier regression was fitted to nighttime net ecosystem exchange (NEE) series, which is assumed to be representative of ecosystem respiration (R_{eco}), using the method proposed by Richardson & Hollinger (2005):

$$R_{eco} = f_0 + s_1 \times \sin(D_\pi) + c_1 \times \cos(D_\pi) + s_2 \times \sin(2 \times D_\pi) + c_2 \times \cos(2 \times D_\pi) + \varepsilon \qquad (4)$$

where f_0, s_1, c_1, s_2 and c_2 are Fourier fitted coefficients, $D_\pi = DOY \times 360 / 365$ (DOY: Day of Year), and ε is the regression residuals. We used this method due to its minimal use of environmental covariates to compute R_{eco} (Richardson & Hollinger 2005). GPP were then derived as $GPP = R_{\mathrm{eco}} - NEE$. As the intent of this study was to obtain a reliable time series of GPP observations to compare with satellite observations, we computed 8-day average GPP to match the temporal resolution of MODIS products.

2.3 Satellite data

2.3.1 MODIS surface reflectances and vegetation indices

Approximately 13.5 years (February 2000 – July 2013) of 8-day 500 m Surface Reflectance product (MOD09A1, Collection 5, tiles h30v10 and h30v11) (Vermote et al., 2002) was obtained through the online Data Pool at the NASA Land Processes Distributed Active Archive Centre (LP DAAC), USGS/Earth Resources Observation and Science (EROS) Centre, Sioux Falls, South Dakota (https://lpdaac.usgs.gov/data_access). A 3 × 3 MOD09A1 500 m pixel window (2.25 km^2) was used to extract the reflectances time series to match the footprint of EC towers and to compute the vegetation indices. Within the extracted reflectance time series, we selected data satisfying all of the following conditions based on the 16-bit QC (500 m state flags) and 32-bit QC (500 m reflectance band quality) layers provided along with MOD09A1: (1) corrected product produced at ideal quality all bands; (2) highest quality for band 1-7; (3) atmospheric correction performed; (4) adjacency correction performed; (5) MOD35 cloud flag indicate "clear"; (6) no cloud-shadow was detected; (7) low or average aerosol quantities.

NDVI and EVI are widely used as proxies of canopy "greenness", an integrative composite property of green leaf area, green foliage cover, structure, and leaf chlorophyll content (Myneni et al., 1995). VIs are robust and seamless biophysical measures, computed identically across all pixels in time and space regardless of biome type, land cover condition, and soil type (Huete & Glenn, 2011). EVI was used as an optimized version of NDVI that effectively reduces soil background influences and atmospheric noise variations (Huete et al., 2002). The equations defining NDVI (Tucker, 1979) and EVI are:

$$\mathrm{NDVI} = \frac{\rho_{\mathrm{nir}} - \rho_{\mathrm{red}}}{\rho_{\mathrm{nir}} + \rho_{\mathrm{red}}}$$

$$\mathrm{EVI} = 2.5\frac{\rho_{\mathrm{nir}} - \rho_{\mathrm{red}}}{\rho_{\mathrm{nir}} + 6\rho_{\mathrm{red}} - 7.5\rho_{\mathrm{blue}} + 1} \quad (5)$$

where ρ_{nir}, ρ_{red} and ρ_{blue} are reflectances of the near infrared (841 – 876 nm), red (620 – 670 nm), and blue (459 – 479 nm) bands of the MODIS sensor, respectively. Hereafter we will refer NDVI and EVI derived from MOD09A1 reflectances specifically as $\mathrm{NDVI}_{\mathrm{MOD09}}$ and $\mathrm{EVI}_{\mathrm{MOD09}}$, respectively.

2.3.2 MODIS GPP product (GPP_{MOD17})

We used the global 1-km 8-day MODIS GPP product (MOD17A2, Collection 055, tiles h30v10 and h30v11) from January 2000 through December 2012 obtained from NASA LP DAAC and USGS EROS repository (https://lpdaac.usgs.gov/data_access) (Running et al., 2004). The algorithm calculates daily GPP as a function of incoming solar radiation, conversion coefficients, and environmental stresses (Running et al., 2004). We used a 1 km^2 window to extract MOD17A2 GPP time series for each flux tower. We used the QA layers embedded in the MOD17A2 product to select data satisfying all the following: (1) MODLAND_QC bits indicate good quality; (2) detectors apparently fine for up to 50% of channels 1, 2; (3) no significant clouds present (clear).

2.3.3 MODIS LAI/fAPAR products (LAI_{MOD15} and $fAPAR_{MOD15}$)

For comparison, we also obtained MODIS 8-day global 1-km LAI/fAPAR product (MOD15A2, Collection 5, tiles h30v10 and h30v11) from February 2000 to May 2013 (Myneni et al., 2002) through NASA LP DAAC and USGS EROS repository (https://lpdaac.usgs.gov/data_access). The main algorithm for retrieval LAI/fAPAR is based on a biome specific lookup table (LUT), which is generated using a three-dimensional radiative transfer (RT) model or using vegetation indices when the main algorithm failed (Myneni et al., 2002). For each field site, a 1 km^2 window was applied to obtain the LAI_{MOD15} and $fAPAR_{MOD15}$ time series. Within the extracted time series, we selected the data satisfying all of the following conditions (1) main (RT) algorithm used, best results possible (no saturation); (2) significant clouds not present (clear); (3) no or low atmospheric aerosol.

2.3.4 MODIS LST product, daytime (LST_{MOD11})

We obtained 1-km 8-day MODIS global land surface temperature (LST) product (MOD11A2, Collection 5, tiles h30v10 and h30v11) from NASA LP DAAC and USGS EROS repository (https://lpdaac.usgs.gov/data_access). The MOD11 LST product was generated based on the generalized split-window algorithm (Wan & Dozier, 1996). At each flux tower, we applied a 1 km^2 window to obtain the daytime LST_{MOD11} time series. We selected the LST_{MOD11} observations satisfying all the following conditions: (1) LST produced with good quality; (2) good data quality of L1B in 7 TIR (thermal infrared) bands; (3) average emissivity error <= 0.02; (4) average LST error <= 2K.

2.4 Variations of EVI-based GPP models

We also compared the performances of two variations of EVI-based GPP models, namely the T-G (Temperature and Greenness) model (Sims et al., 2008) and G-R (Greenness and Radiation) model (Gitelson et al., 2006).

2.4.1 Temperature - Greenness model

The T-G model was formulated as (Sims et al., 2008):

$$\mathrm{GPP} \propto \mathrm{EVI_{scaled}} \times \mathrm{LST_{scaled}} \quad (6)$$

where the EVI_{scaled} was calculated following Sims et al. (2008):

$$\mathrm{EVI_{scaled}} = \mathrm{EVI} - 0.1 \tag{7}$$

The LST_{scaled} can be computed as (Sims et al., 2008):

$$\mathrm{LST_{scaled}} = \min[(\mathrm{LST}/30); (2.5 - (0.05 \times \mathrm{LST}))] \tag{8}$$

LST_{scaled} sets GPP to zero when LST is less than zero and thus defines the inactive winter period (Sims et al., 2008). LST_{scaled} also accounts for low temperature limitations to photosynthesis when LST is between 0 and 30 °C, as well as accounts for high temperature and high VPD stress in sites that exceed LST values of 30 °C (Sims et al., 2008).

2.4.2 Greenness - Radiation model

The G-R model was formulated as (Gitelson et al., 2006; Peng et al., 2013):

$$\mathrm{GPP} \propto \mathrm{VI_{chl}} \times \mathrm{PAR_{TOC}} \tag{9}$$

where VI_{chl} is the chlorophyll-related spectral index. We used EVI as VI_{chl} following Wu et al. (2011). PAR_{TOC} is the tower measured PAR incident at the top-of-canopy (MJ m^{-2} d^{-1}), computed as 50% of the tower measured shortwave incoming radiation (MJ m^{-2} d^{-1}) following Papaioannou et al. (1993).

PAR_{TOC} can be obtained at flux tower sites, but not across the entire region. Therefore, in addition to the original G-R model driven by PAR_{TOC}, we also proposed a modified version by replacing PAR_{TOC} with PAR incident at the top-of-atmosphere (PAR_{TOA}) to extrapolate beyond the tower footprint. The modified G-R model is formulated as:

$$\mathrm{GPP} \propto \mathrm{EVI} \times \mathrm{PAR_{TOA}} \tag{10}$$

where PAR_{TOA} is the top-of-atmosphere PAR (MJ m^{-2} d^{-1}), computed as the 40% of top-of-atmosphere incoming solar radiation (R_{TOA}, MJ m^{-2} d^{-1}) following Monteith & Unsworth

(2013). R_{TOA}, also known as extraterrestrial radiation, is the amount of global horizontal radiation that a location on Earth would receive if there was no atmosphere or clouds (i.e., in outer space). The R_{TOA} can be computed from Earth-Sun geometry:

$$\mathrm{R_{TOA}} = \frac{\mathrm{S_0}}{\pi}\left(\frac{\mathrm{r_0}}{\mathrm{r}}\right)^2 (\mathrm{H}\sin\phi\sin\delta + \sin\mathrm{H}\cos\phi\cos\delta) \tag{11}$$

where S_0 is solar constant (1366 W m^{-2} or 118.02 MJ m^2 d^{-1}); r is the Earth-Sun distance; r_0 is the mean Earth-Sun distance; H is sun hour angle at sunset; ϕ is latitude (°); and δ is solar declination (°).

The PAR_{TOA} used in this study is essentially similar to the potential PAR ($PAR_{potential}$, the maximal PAR when atmospheric gases and aerosols are minimal) proposed by Gitelson et al. (2012), as both replace site-based measures of PAR_{TOC} to estimate GPP based on solely remote sensing data and reduce the uncertainties associated with high frequency fluctuations of PAR_{TOC} that result in noises and not affect plant photosynthesis (Gitelson et al., 2012; Peng et al., 2013). It should be noted that the computation of $PAR_{potential}$ requires long term PAR_{TOC} measurements for calibration purposes (Gitelson et al., 2012; Peng et al., 2013), or being modelled using 6S (Second Simulation of a Satellite Signal in the Solar Spectrum) radiative transfer code (Kotchenova & Vermote, 2007; Vermote et al., 1997), or modelled from a look-up table method (Lyapustin, 2003). In contrast, the computation of PAR_{TOA} only requires several readily available variables such as date and latitude, thereby eliminating the need for long-term PAR_{TOC} measurements or use of more complicated algorithms to facilitate the extension from flux tower to regional scales.

2.5 Ecosystem light-use-efficiency model

Traditional LUE models require separate estimations of fAPAR and ε for estimation of GPP. However, the coupling of EVI × PAR_{TOC} (Eq. 9) for estimating GPP implies that EVI can be more explicitly used as a measure of ecosystem light-use-efficiency (eLUE), defined as the ratio between GPP and PAR_{TOC}:

$$\mathrm{eLUE_{TOC}} = \frac{\mathrm{GPP}}{\mathrm{PAR_{TOC}}} = f(\mathrm{EVI}) \tag{12}$$

where $eLUE_{TOC}$ (g C MJ^{-1}) was computed for each site using 8-d average GPP (g C m^{-2} d^{-1}) and 8-d average PAR_{TOC} (MJ m^{-2} d^{-1}); *f*(EVI) was obtained through the regression of $eLUE_{TOC}$ against EVI. Once the $eLUE_{TOC}$ was estimated, an eLUE model for predicting GPP driven by PAR_{TOA} is formulated as:

$$\mathrm{GPP} = \mathrm{eLUE_{TOC}} \times \mathrm{PAR_{TOC}} \tag{13}$$

Similarly, the eLUE can also be defined as the ratio between GPP and PAR_{TOA} (Eq. 10):

$$\mathrm{eLUE_{TOA}} = \frac{\mathrm{GPP}}{\mathrm{PAR_{TOA}}} = f(\mathrm{EVI}) \tag{14}$$

where $eLUE_{TOA}$ (g C MJ^{-1}) was computed for each site using 8-d average GPP (g C m^{-2} d^{-1}) and 8-d average PAR_{TOA} (MJ m^{-2} d^{-1}); *f*(EVI) was obtained through the regression of $eLUE_{TOA}$ against EVI. Once the $eLUE_{TOA}$ was estimated, an eLUE model for predicting GPP driven by PAR_{TOA} can be formulated as:

$$\mathrm{GPP} = \mathrm{eLUE_{TOA}} \times \mathrm{PAR_{TOA}} \tag{15}$$

To establish the relationship between eLUE and EVI (i.e., to calibrate the eLUE model) and provide independent validation, the dataset from all four NATT sites (354 samples) were first randomized and then divided equally into two subsets, namely calibration dataset (177 samples) and validation dataset (177 samples) respectively. The GPP_{MOD17} dataset was also divided into calibration and validation subsets only for comparison with the other three EVI-based GPP models.

2.6 Data analysis and statistics

Due to data gaps in satellite observations and EC tower measurements, an immediate comparison of the correlations between satellite indices/products and GPP_{EC} may result in biased conclusions due to different subsets of observations. For examples, the proportion of 8-day gaps across four NATT sites in LAI_{MOD09}, GPP_{MOD17}, EVI_{MOD09} and GPP_{EC} were 22%, 16%, 12% and 21% respectively. To achieve a more valid comparison of the performances of satellite indices in tracking seasonal variations in GPP_{EC}, we removed the tower observations corresponding to satellite index or PAR measurements missing for a particular site-date. Thus, comparisons among all satellite indices as well as variations of EVI-based GPP models were based on exactly the same subset of GPP_{EC} measurements across 4 EC flux tower sites (total of 354, 8-day samples).

To assess the performances for up-scaling the tower derived GPP across biological phenophases, the dataset of each site was further divided into two subsets, namely the green-up phase subset and brown-down phase subset. The green-up phase was defined as the period from minimum GPP preceding the growing season to the peak (maximum GPP), and the brown-down phase was defined as the subsequent period from peak to minimum GPP, (i.e., following the cessation canopy greening).

We used three tests to compare the predictions of satellite indices/products to GPP_{EC}. First, the coefficient of determination (R^2) was computed using the ordinary least-squares (OLS) algorithm to measure the variance of GPP_{EC} that is explained by the satellite indices/products. Second, the analysis of covariance (ANCOVA) was then used to test the significance of the differences in linear regression slope and intercept between regression models. Third, we calculated the root mean squared error (RMSE) between measured and modelled GPP values to assess the model accuracy:

$$\text{RMSE} = \sqrt{\frac{\sum_{t=1}^{n} (Obs - Pred)^2}{n}} \tag{16}$$

where *Obs* is the tower measured GPP, *Pred* is the satellite estimated GPP.

We computed the coefficient of variation (CV) for quantifying the inter-annual variations in GPP. The CV can be computed as:

$$\text{CV} = \frac{\sigma}{|\mu|} \times 100 \tag{17}$$

where σ is standard deviation of annual GPP (g C m^{-2} yr^{-1}), $|\mu|$ is the absolute value of the mean annual GPP (g C m^{-2} yr^{-1}). Data processing, statistical analysis and visualization were performed in R scientific computation environment (version 3.0.2, R Core Team, 2013) and associated packages contributed by user community (http://cran.r-project.org).

3 Results

3.1 Performances of satellite products and models in tracking tower GPP

The scatter plots between MODIS vegetation products and GPP_{EC} for each of the four individual NATT flux tower sites are shown in Figure 2. $fAPAR_{MOD15}$ and GPP_{MOD17} were only moderately correlated with GPP_{EC}, with R^2 values of GPP_{MOD17} less than 0.40 at three of the 4 sites (Fig. 2B - C; Table 2). $NDVI_{MOD09}$ relationships with GPP_{EC} were overall slightly improved or equivalent to those of $fPAR_{MOD15}$ (Fig. 2D, Table 2). In contrast, LAI_{MOD15} and EVI_{MOD09} were much more strongly correlated with GPP_{EC}, with R^2 values between 0.60 and 0.90 (Figs. 2A, E; Table 2). The EVI_{MOD09} was slightly more stable across all individual sites with R^2 larger than 0.66 at all sites (Fig. 2E; Table 2).

A cross-site analysis showed that $NDVI_{MOD09}$, $fAPAR_{MOD15}$, and GPP_{MOD17} could explain 77% ($F(1, 352) = 1197$, $p < 0.0001$), 72% ($F(1, 352) = 919.8$, $p < 0.0001$) and 58% (F(1,

352) = 491.2, $p < 0.0001$) of the seasonal variation in GPP_{EC} respectively (Fig. 3B - D; Table 2). In comparison, LAI_{MOD15} and EVI_{MOD09} explained 80% ($F(1, 352) = 1412$, $p < 0.0001$) and 84% ($F(1, 352) = 1871$, $p < 0.0001$) of seasonal variation in GPP_{EC}, respectively (Fig. 3A, E; Table 2). Overall, the EVI_{MOD09} and LAI_{MOD15} products were found to be the best satellite measures for both individual-site and cross-site estimations of GPP_{EC} and thus for regional scaling along the NATT study area, we continued our analysis using the slightly better performing EVI_{MOD09}.

The coupling of EVI with LST_{scaled} in the T-G model resulted in no improvement in correlations with GPP_{EC} compared to EVI_{MOD09} alone for all sites (cf. Figs. 2E and 4A). In contrast, coupling of EVI with PAR_{TOC} in the G-R model did improve correlations at Adelaide River ($R^2 = 0.86$, $F(1, 41) = 245$, $p < 0.0001$) and Ti Tree sites ($R^2 = 0.79$, $F(1, 85) = 317.2$, $p < 0.0001$) (cf. Figs. 2E and 4B) relative to EVI_{MOD09} alone. The coupling EVI with PAR_{TOA} (top-of-atmosphere PAR) resulted in further improvements over all sites, with R^2 values between 0.78 to 0.89 over the different savanna vegetation classes and climatic conditions (cf. Figs. 2E and 4C).

In the cross-site analyses, the T-G model decreased the R^2 to 0.81 ($F(1, 352) = 1482$, $p < 0.0001$) compared with EVI_{MOD09} alone (cf. Figs. 3E and 5A), while the G-R models improved the R^2 to 0.85 ($F(1, 352) = 1964$, $p < 0.0001$) and 0.87 ($R^2 = 0.87$, $F(1, 352) = 2276$, $p < 0.0001$) for PAR_{TOC} and PAR_{TOA} respectively (cf. Figs. 3E and 5B, C).

3.2 eLUE models for up-scaling tower GPP

We examined the use of EVI_{MOD09} as a measure of eLUE (defined as GPP/PAR) and analyzed the direct relationships between eLUE and EVI_{MOD09} for the PAR_{TOC} ($eLUE_{TOC}$) and PAR_{TOA} ($eLUE_{TOA}$) definitions. Figure 6 presents the cross-site relationships between eLUE and EVI_{MOD09} for the calibration and validation datasets, respectively. The regression coefficients and predictive errors are summarized in Table 3. Overall, EVI_{MOD09} correlated strongly with both $eLUE_{TOC}$ (R^2 = 0.84, $F(1, 175)$ = 902.7, p < 0.0001, RMSE = 0.0733 g C m^{-2} MJ^{-1}) and $eLUE_{TOA}$ (R^2 = 0.81, $F(1, 175)$ = 1003, p < 0.0001, RMSE = 0.0534 g C m^{-2} MJ^{-1}) in the calibration dataset (Fig. 6, Table 4). Likewise in the validation dataset, EVI_{MOD09} showed a strong correlation with $eLUE_{TOC}$ (R^2 = 0.84, $F(1, 175)$ = 894.3, p < 0.0001, RMSE = 0.0753 g C m^{-2} MJ^{-1}) and $eLUE_{TOA}$ (R^2 = 0.85, $F(1, 175)$ = 1003, p < 0.0001, RMSE = 0.0500 g C m^{-2} MJ^{-1}) (Fig. 6, Table 3), suggesting that spatial and seasonal variations in eLUE can be captured by EVI_{MOD09} across the NATT sites.

The cross-site linear regression model for calculation of $eLUE_{TOC}$ using EVI_{MOD09} was obtained from the calibration dataset as:

$$\mathrm{eLUE_{TOC}} = 1.78 \times (\mathrm{EVI_{MOD09}} - d) \tag{18}$$

where d (0.08) is an offset to subtract the contribution of soil background and adjust EVI_{MOD09} to zero when GPP is 0 g C m^{-2} d^{-1} estimated through inversion of the cross-site GPP_{EC} ~ EVI_{MOD09} linear regression model. The cross-site linear regression model for calculation of $eLUE_{TOA}$ using EVI was obtained from the calibration dataset as:

$$\mathrm{eLUE_{TOA}} = 1.17 \times (\mathrm{EVI_{MOD09}} - d) + 0.03 \tag{19}$$

Consequently, a model for calculating GPP using $eLUE_{TOC}$ and PAR_{TOC} can be constructed in the sense of the eLUE concept as:

$$\mathrm{GPP} = \overbrace{[1.78 \times (\mathrm{EVI_{MOD09}} - 0.08)]}^{\mathrm{eLUE_{TOC}}} \times \mathrm{PAR_{TOC}} \tag{20}$$

Similarly, a model for calculating GPP using $eLUE_{TOA}$ and PAR_{TOA} can be constructed as:

$$\mathrm{GPP} = \overbrace{[1.17 \times (\mathrm{EVI}_{\mathrm{MOD09}} - 0.08) + 0.03]}^{\mathrm{eLUE}_{\mathrm{TOA}}} \times \mathrm{PAR}_{\mathrm{TOA}} \quad (21)$$

Equations 20 and 21 represent two savanna landscape GPP models that use either PAR_{TOC} or PAR_{TOA} in combination with EVI_{MOD09} parameterized eLUE as model input. Hereafter we will refer Eqs. 20 and 21 as $eLUE_{TOC}$ and $eLUE_{TOA}$ models, respectively.

Figure 7 presents the cross-site relationships between GPP_{EC} and GPP predicted from the eLUE models for the calibration dataset and validation dataset. For comparison, we also present the GPP_{MOD17} and GPP simulated from the EVI_{MOD09} alone (GPP_{EVI}). The model for calculating GPP_{EVI}, i.e., $GPP_{EVI} = (EVI_{MOD09} – 0.08) \times 18.6$, was derived from the linear regression between GPP_{EC} and EVI_{MOD09} using calibration dataset.

Overall, the $eLUE_{TOC}$ and $eLUE_{TOA}$ models demonstrated better performance in predicting GPP_{EC} than GPP_{MOD17} or GPP_{EVI} (Fig. 7; Table 4). In the validation dataset, the R^2 between GPP_{EC} and GPP predicted using the $eLUE_{TOC}$ model ($GPP_{eLUE\text{-}TOC}$) was 0.85 ($F(1, 175) = 1017$, $p < 0.0001$, RMSE = 0.76 g C m^{-2} d^{-1}) (Fig. 7C; Table 4). The correlation between GPP_{EC} and GPP predicted using the $eLUE_{TOA}$ model ($GPP_{eLUE\text{-}TOA}$) was better than the $eLUE_{TOC}$ model, with R^2 of 0.88 ($F(1, 175) = 1297$, $p < 0.0001$, RMSE = 0.70 g C m^{-2} d^{-1}) (Fig. 7D; Table 4). The GPP model based on EVI_{MOD09} alone also performed fairly well for the validation dataset ($R^2 = 0.85$, $F(1, 175) = 978.6$, $p < 0.0001$, RMSE = 0.78 g C m^{-2} d^{-1}), suggesting that EVI_{MOD09}, as a measure of eLUE, can explain a large proportion of variations in GPP_{EC}. In contrast, the predictive power of GPP_{MOD17} to GPP_{EC} is weak and with lower accuracy ($R^2 = 0.58$, $F(1, 175) = 240$, $p < 0.0001$, RMSE = 1.43 g C m^{-2} d^{-1}; Fig. 7A; Table 4).

Figure 8 presents a comparison of time series among satellite and tower derived GPP ($GPP_{eLUE\text{-}TOC}$, $GPP_{eLUE\text{-}TOA}$, GPP_{MOD17} and GPP_{EC}) at the four flux tower sites. Both the

$GPP_{eLUE-TOC}$ and $GPP_{eLUE-TOA}$ matched the seasonal progression of GPP_{EC} quite well (Fig. 8). At the Howard Springs and Daly River sites (*Eucalyptus* woodlands), $GPP_{eLUE-TOA}$ overestimated GPP_{EC} during the dry season in some, but not all years (Fig. 8A-C). GPP_{MOD17} tended to underestimate productivity during the late dry season to early wet season, except in the *Acacia* woodland (Ti Tree) where underestimation occurred during the wet season (Fig. 8). The *Acacia* woodland was also distinct among the NATT sites with GPP_{eLUE} and GPP_{MOD17} failing to capture the largest and smallest values of GPP_{EC} (Fig. 8E).

3.3 Extension of tower GPP across biologic phenophases

Figure 9 presents the site-level relationships between satellite derived GPP and GPP_{EC} partitioned between green-up and brown-down phenophases, respectively over the four NATT sites. The phenophase period showed different relationships between satellite derived GPP and GPP_{EC} over the different NATT sites (Fig. 9). At Howard Springs, the slope of the GPP_{EC} ~ GPP_{MOD17} relationship during the green-up phase was not significantly different ($F(1, 103) = 0.296$, $p = 0.588$) from the slope during the brown-down phase, however, there was a very strong offset bias from the 1:1 symmetry line, with the intercept of the green-up relationships (3.20) significantly higher ($F(1, 103) = 64.04$, $p < 0.001$) than the intercept of the brown-down relationship (1.29) (Fig. 9A). At Daly River, the green-up intercept (2.47) was also significantly higher ($F(1, 115) = 8.13$, $p < 0.001$) than the brown-down intercept (1.48), although the slope was not significantly different between phenophases ($F(1, 115) = 2.54$, $p = 0.114$) (Fig. 9A). At Adelaide River, the green-up slope was significantly smaller than the brown-down slope ($F(1, 40) = 4.54$, $p = 0.040$) (Fig. 9A), while the difference between phenophase responses (i.e., the slope of the GPP_{EC} ~ GPP_{MOD17} relationship) was most pronounced at the Ti Tree site ($F(1, 85) = 18.92$, $p < 0.001$) (Fig. 9A).

Phenophase dependent bias was reduced in the GPP_{EC} ~ GPP_{EVI} relationships, but remained significant at Howard Springs ($F(1, 103) = 7.42$, $p = 0.008$), Daly River ($F(1, 115) = 8.08$, $p = 0.005$), and Ti Tree ($F(1, 85) = 5.03$, $p = 0.024$), while phenophase slopes were not significantly different at Adelaide River ($F(1, 40) = 2.52$, $p = 0.121$) (Fig. 9B).

Phenophase differences were reduced further, but not removed altogether, by use of the eLUE models (Fig 9C, D). In the GPP_{EC} ~ $GPP_{eLUE\text{-}TOC}$ relationships, phenophase-dependent slopes were not significantly different at Adelaide River ($F(1, 40) = 0.73$, $p = 0.400$) and Ti Tree ($F(1, 85) = 0.75$, $p = 0.389$), but maintained slope differences at Howard Springs ($F(1, 103) = 10.27$, $p = 0.002$) and Daly River ($F(1, 115) = 14.91$, $p < .001$) (Fig. 9C). In the GPP_{EC} ~ $GPP_{eLUE\text{-}TOA}$ relationships, the phenophase slopes were significantly different at Daly River ($F(1, 115) = 6.30$, $p = 0.005$), Howard Springs ($F(1, 103) = 4.94$, $p = 0.029$) and marginally significant at Adelaide River ($F(1, 40) = 4.14$, $p = 0.049$), while not significantly different at Ti Tree ($F(1, 85) = 3.57$, $p = 0.069$) (Fig. 9D).

3.4 Biogeographic patterns of savanna GPP over the NATT study area

Figure 10 illustrates the strong control by rainfall of the spatial and temporal biogeographic patterns of savanna GPP simulated using the $eLUE_{TOA}$ model (Eq. 21) over the NATT study area. Mean annual GPP decreased from 1400 g C m^{-2} yr^{-1} to less than 400 g C m^{-2} yr^{-1} from the northern humid region to southern xeric inland (Fig. 10A). Associated with decreasing mean annual GPP, inter-annual variation in GPP, quantified as the coefficient of variation (CV) of GPP, was generally less than 10% over most northern humid forests and woodlands but increased to more than 30% over the southern xeric grasslands and shrublands (Fig. 10B).

Figure 10 also presents a comparison of biogeographic patterns of savanna GPP between wet (January - March) and dry (July - September) seasons. From north to south, the mean daily GPP during the wet season decreased by 66% from more than 6 g C m^{-2} d^{-1} in the coastal, humid regions dominated by *Eucalyptus* forests and woodlands to less than 2 g C m^{-2} d^{-1} over the southern, xeric areas, where hummock grasslands and *Acacia* woodlands and shrublands were the dominant vegetation types (Fig. 10C). However, during the dry season, GPP was small with little spatial variability (Fig. 10D). Region-wide mean daily GPP during the wet season (2.94±1.44 g C m^{-2} d^{-1}) was almost 2 times larger than the mean daily GPP for the dry season (1.48±0.61 g C m^{-2} d^{-1}), reflecting the large impacts of seasonal rainfall distribution on savanna GPP.

4 Discussion

4.1 Tracking EC tower derived GPP with satellite observations

We found that among five satellite vegetation products, EVI correlated best to EC flux tower derived GPP (GPP_{EC}) across the four mesic-to-arid NATT sites (R^2 = 0.84; Fig. 3). This was further improved by coupling EVI with PAR_{TOC} (R^2 = 0.85; Fig. 5B) or PAR_{TOA} (R^2 = 0.87; Fig. 5C), enabling EVI to be used as a measure of eLUE (GPP/PAR). Two savanna landscape eLUE models parameterized with EVI and driven by PAR_{TOC} or PAR_{TOA}, were further analyzed (the $eLUE_{TOC}$ and $eLUE_{TOA}$ models respectively) for estimation of GPP. The eLUE models resulted in improved GPP predictions across the mesic and xeric savanna sites, suggesting that region-wide GPP can be predicted with reasonable accuracy from purely satellite remote sensing observations without dependence on interpolated ground meteorology.

We found that GPP_{MOD17} was only moderately correlated with GPP_{EC} (R^2 = 0.58). All other satellite products (except $fAPAR_{MOD15}$ at Howard Springs) showed much better performances than GPP_{MOD17} in tracking GPP_{EC}. As $fAPAR_{MOD15}$ was better correlated to GPP_{EC} than GPP_{MOD17} (cf. Fig. 2B and C), the introduction of meteorological inputs into GPP_{MOD17}

degraded the correlation between GPP_{MOD17} and GPP_{EC}, demonstrating some of the difficulties in accurate estimations of LUE at landscape scales (Kanniah et al., 2009; Sjöström et al., 2013).

Coupling EVI with temperature and radiation measures showed mixed results in predicting savanna GPP. There were no improvements in using the Temperature-Greenness (T-G) model ($EVI_{scaled} \times LST_{scaled}$) for predicting GPP compared with using EVI alone over the NATT study area (cf. Figs. 2E and 4A). This may be due to temperature not being a limiting factor or significant driver of photosynthesis in tropical savannas (Leuning et al., 2005; Kanniah et al., 2009; Cleverly et al., 2013), or that LST_{scaled} was not an appropriate surrogate for radiation. In contrast, we found significant improvements with use of the Greenness-Radiation (G-R) models (EVI × PAR) for predicting GPP_{EC}, relative to EVI alone (cf. Fig. 2E to Figs. 4B and 4C), reflecting the importance of the quantity of radiation as a critical driver of savanna vegetation productivity (Whitley et al., 2011; Kanniah et al., 2013).

We found that coupling EVI with PAR_{TOA} better predicted GPP than coupling EVI with PAR_{TOC} (cf. Figs. 4B and 4C). This was not necessarily expected as theoretically, tower measured PAR incident at the top-of-canopy (PAR_{TOC}) should be preferable since it considers diurnal and seasonal variations in local weather conditions. Some studies made over various cropland and grassland flux tower sites have also found that coupling EVI with potential PAR (maximal value of PAR_{TOC}) provided better accuracy in predicting GPP than coupling EVI with PAR_{TOC} (Gitelson et al., 2012; Peng et al., 2013; Rossini et al., 2014). Gitelson et al. (2012) attributed the better performance of $PAR_{potential}$ instead of actual PAR_{TOC} due to the saturation of GPP vs. PAR_{TOC} relationship in soybean cropland, noting that a decrease in PAR_{TOC} may not correspond to a decrease in GPP. Over north Australian savannas, Kanniah et al. (2013) found that the negative effect of decreases in PAR_{TOC} due to wet season cloud cover on rates of photosynthesis were partly compensated by enhanced ε due to the increased proportion of diffuse radiation. Therefore, multiplying EVI by PAR_{TOA} may mimic $PAR_{potential}$ and better approximate radiation controls on GPP.

4.2 Phenophase impacts on the up-scaling of GPP across seasons

Large discrepancies in the relationship between GPP_{MOD17} and GPP_{EC}, and smaller but significant differences in the relationships between GPP_{EVI} and GPP_{EC}, were found between green-up and brown-down phenophases at all NATT study sites, particularly at the xeric Ti Tree site (Fig. 9). Phenophases relationships differed in their intercepts and slopes and also showed strong nonlinearities during the brown-down phase (Fig. 9). By contrast, the phenophase-dependencies on the up-scaling of GPP were minimized with the use of eLUE models, with the inclusion of PAR greatly reducing seasonal hysteresis at the Adelaide River and Ti Tree sites (Fig. 9D).

This reduction of hysteresis in the eLUE model was quite intriguing and is mostly likely explained by the differing light conditions encountered between the green-up and brown-down phases. For example, during the green-up at Ti Tree (Nov 2010 - Feb 2011), mean PAR_{TOC} and PAR_{TOA} were 12.82 MJ m^{-2} d^{-1} and 16.61 MJ m^{-2} d^{-1} respectively, while in contrast mean PAR_{TOC} and PAR_{TOA} during brown-down (March to July 2011) were 9.11 MJ m^{-2} d^{-1} and 11.11 MJ m^{-2} d^{-1}, representing a 29% and 33% reduction in PAR_{TOC} and PAR_{TOA}, respectively, during the brown-down phase and hence resulting in a different radiation environment across phenophases. Therefore, equal values of EVI, in green-up and brown-down phases, may result in differing GPP values due to differences in radiation (duration and intensity). Such differences in light conditions across seasonal phenophases are largely normalized in eLUE (GPP / PAR).

The use of eLUE, and in particularly PAR_{TOA}, may also correct for photoperiod effects on photosynthetic capacity. In a recent study, Bauerle et al. (2012) reported that photoperiod explained more seasonal variation in photosynthetic capacity across 23 tree species than temperature, and suggested that photoperiod-associated declines in photosynthetic capacity could limit autumn carbon gain in forest, even under favorable autumn conditions. Since photoperiod (day length) is near-linearly correlated with PAR_{TOA} ($R^2 = 0.95$, $F(1, 4352)$, $p < 0.0001$), its incorporation in an eLUE model will potentially correct for photoperiod effects on photosynthetic capacity. However, this would require much further analysis to assess the extent to which there is a response of photosynthetic capacity to variations in photoperiod in tropical savannas.

The moisture stress during the browning phenophase may explain some of the residual seasonal hysteresis on the GPP_{EC} ~ $GPP_{eLUE\text{-}TOA}$ relationship. Across the NATT EC flux tower sites, rainfall ends in March-April followed by large vapor pressure deficits (VPD) and decreasing soil moisture from April through to September (Eamus et al., 2013), coincident with the brown-down phase of GPP at these sites. Whereas, declines in GPP_{EC} arise rapidly from stomatal closure during the brown-down phase, chlorophyll degradation and/or the loss of LAI are slower processes that take place at longer time scales (Huemmrich et al., 2005; Jenkins et al., 2007; Ma et al., 2013). Future studies can investigate if the phenophase phase dependency could be further reduced by inclusion of a soil moisture term in the eLUE model to account the rapid declines in photosynthesis associated with stomatal closure.

Despite the differences in relationships for green-up and brown-down phases, for the entire growing season, EVI explained 66% variances of GPP_{EC} variations at Ti Tree site, while incorporation of PAR_{TOC} and PAR_{TOA} (i.e., the eLUE models) increased the R^2 to 0.79 and 0.80 respectively. This suggested that the eLUE models are able to provide reasonable estimates of GPP at the southern xeric savannas where both species composition and climatic conditions are quite different from the northern mesic savannas.

4.3 EVI as a measure of ecosystem light-use-efficiency (eLUE)

It was encouraging to see that coupling EVI with the radiation driver, PAR, provided a better estimation of GPP across the savanna study sites. With the rate of photosynthesis, GPP, defined as the product of fAPAR, ε and PAR (Monteith ,1972), then the coupling of EVI with eLUE (or GPP / PAR) means that EVI, a greenness index, becomes a function as the product of fAPAR and ε, as

$$\frac{\mathrm{GPP}}{\mathrm{PAR}} = \mathrm{eLUE} \sim f(\mathrm{EVI}) = \mathrm{fAPAR} \times \varepsilon \tag{22}$$

Historically, the linear relationships between VIs and fAPAR have been well documented through theoretical analyses (Sellers, 1985, 1987; Carlson & Ripley, 1997), field measurements (Ruimy et al., 1994; Gamon et al., 1995; Fensholt et al., 2004), and radiative transfer models (Carlson & Ripley, 1997; Goward & Huemmrich, 1992; Myneni & Williams, 1994). However, if EVI only represents fAPAR, then it is not enough to explain the strong relationship between EVI and eLUE, unless (1) the temporal variations in ε are very small, or (2) the temporal variations in fAPAR and ε are synchronized.

However, it is well known that ε varies widely across seasons (Sims et al., 2006; Jenkins et al., 2007) and under different types of environmental stress (Ruimy et al., 1995). This can be further confirmed by previous studies that have shown that savanna ecosystems in northern Australia utilize radiation more efficiently in the wet season than in the dry season, therefore ε exhibiting strong seasonality (Fordyce et al., 1995; Eamus & Cole, 1997; Kanniah et al., 2009; Eamus et al., 2013). These studies argue against the first hypothesis that temporal variations in ε are very small, and hence cannot explain the strong correlation between eLUE and EVI.

The alternative explanation is that the temporal variations in fAPAR and ε are synchronized and hence both are correlated with EVI. In fact, Sims et al. (2006) reported that ε derived from nine flux towers in North America was strongly correlated to EVI ($R^2 = 0.76$). Wu et al. (2012) reported moderate correlation between EVI and tower ε in temperate and boreal forest ecosystems in North America. On the other hand, such relationships were weaker in evergreen forests relative to deciduous ones and a study in an evergreen oak forest showed no correlation between EVI and ε (Goerner et al., 2009). Thus, we may infer that the correlation between eLUE and EVI is likely due to the synchronization between fAPAR and ε in the ecosystems that the seasonal variations in photosynthesis are primarily driven by dynamics of deciduous species and/or annual species.

Seasonal fAPAR (indicated by LAI) and seasonal ε in northern Australian savannas were found to exhibit similar phenological patterns (Kanniah et al., 2009; Whitley et al., 2011). In Australian tropical savannas, the primary determinant of seasonal variations in leaf area, light interception and canopy gas exchanges is defined by the dynamics of the understorey grasses and forbs, which respond to intra-annual rainfall distribution (Hutley et al., 2001; O'Grady et al., 2009; Eamus et al., 2013; Cleverly et al., 2013). Meanwhile, environmental conditions also become favorable for photosynthesis (high solar radiation, high soil moisture, low VPD) following the onset of the wet season, thus the ε of both C_3 trees and C_4 grasses is larger in the wet season (Fordyce et al., 1995; Eamus & Cole, 1997; Eamus et al., 1999; O'Grady et al., 1999; Prior et al., 1997). Consequently, fAPAR and ε displayed similar phenological patterns in response to changes in environmental factors in north Australian savannas (Williams et al., 1997; O'Grady et al., 2000; Kanniah et al., 2009).

In summary, the tight correlation between eLUE and EVI can be attributed to the fact that EVI is not only related to light absorption capacity (fAPAR), but also integrates the effects of phenological stage and environmental stress on photosynthetic efficiency (ε). Although we could derive fAPAR and ε separately, from a remote sensing perspective these ecosystem variables cannot be directly measured by current satellite sensors. Therefore, EVI tends to be a good composite measure that simplifies the up-scaling of carbon fluxes from flux towers to regional scale. The savanna biome consists of multiple plant functional types (PFTs) and plant function for these different PFTs that are difficult to parameterize due to a complex mixture of distinct physiological characteristics, with fractions of tree (C_3) and grass (C_4) varying across space and time, and each PFT has its own unique relationships with environmental factors (Scholes & Archer, 1997). The eLUE model framework presented here represents a substantial improvement to the current MODIS global GPP product for tropical savannas, an ecosystem that covers one eighth of the global land area (Scholes & Archer, 1997) and contributes approximately 30% of terrestrial ecosystem GPP (House & Hall, 2001).

5 Conclusions

Measurement of landscape carbon fluxes is an essential task in global change studies, yet current production efficiency models parameterize LUE with coarse resolution, interpolated meteorology, which introduces uncertainties that may reduce the confidence in estimated primary production. In searching for a simple GPP model based entirely on satellite remote sensing observations, we found that MODIS EVI had the strongest cross-site relationships with EC tower derived GPP at both mesic and xeric north Australian savannas. This was further improved by coupling EVI with PAR_{TOC} or PAR_{TOA} and using EVI as a measure of eLUE (GPP/PAR). Two simple savanna landscape GPP models based on EVI parameterized eLUEs and driven by PAR_{TOC} or PAR_{TOA} were further analyzed and GPP simulated using these eLUE models agreed well with tower GPP across all sites. We also found that biological phenophase dependency of satellite GPP *versus* tower GPP relationships across green-up and brown-down periods, which was most pronounced for MOD17 GPP, can be considerably reduced by the use of eLUE models. These results suggest that region-wide savanna GPP can be estimated fairly accurately using purely satellite remote sensing observations without dependencies on interpolated ground meteorology nor estimation of ε.

As stated in the beginning, technical approaches of estimating GPP from remote sensing datasets fall into two technical pathways: LUE-based process models and VI-based empirical models. Here we suggest that replacing LUE (GPP/APAR) with eLUE (GPP/PAR), which is parameterized using readily available MODIS EVI, results in convergence of these two technical pathways. The convergence yielded simple, yet reliable estimates of savanna landscape GPP based entirely on satellite remote sensing observations (through the use of PAR_{TOA}), which has potential to be applied over large scales for better assessment of the region-wide savanna carbon dynamics in a truly spatially continuous way.

Acknowledgement

This work was jointly supported by National Basic Research Program of China (No.2012CB955304), Australian Research Council projects ARC-DP140102698, ARC-DP1115479, ARC-DP130101566, and the Chinese Scholarship Council. We thank Drs. Kevin Davies and Rakhesh Devadas for maintaining local remote sensing database and providing e-Research support. We would like to thank all the personnel involved with the operation of the flux towers.

References

Anderson, A. N., Braithwaite, Cook, G. D., Corbett, L. K., Williams, R. J., Douglas, M. M., et al. (1998). Fire research for conservation management in tropical savannas: introducing the Kapalga fire experiment. *Austral Ecology*, 23(2), 95–110.

Baldocchi, D., Falge, E., Gu, L., Olson, R., Hollinger, D., Running, S., et al. (2001). FLUXNET: A New Tool to Study the Temporal and Spatial Variability of Ecosystem-Scale Carbon Dioxide, Water Vapor, and Energy Flux Densities. *Bulletin of the American Meteorological Society*, 82(11), 2415.

Bauerle, W. L., Oren, R., Way, D. A., Qian, S. S., Stoy, P. C., THORNTON, P. E., et al. (2012). Photoperiodic regulation of the seasonal pattern of photosynthetic capacity and the implications for carbon cycling. *Proceedings of the National Academy of Sciences*, 109(22), 201119131–8617.

Beringer, J., Hutley, L. B., Tapper, N. J., & Cernusak, L. A. (2007). Savanna fires and their impact on net ecosystem productivity in North Australia. *Global Change Biology*, 13(5), 990–1004.

Beringer, J., Hacker, J., Hutley, L. B., Leuning, R., Arndt, S. K., Amiri, R., et al. (2011). SPECIAL—Savanna Patterns of Energy and Carbon Integrated across the Landscape. *Bulletin of the American Meteorological Society*, 92(11), 1467.

Borchert, R. (1994). Induction of rehydration and bud break by irrigation or rain in decidous trees of a tropical dry forest in Costa Rica. *Trees*, 8(4).

Canadell, J. G., Pataki, D. E., Gifford, R., Houghton, R. A., Luo, Y., Raupach, M. R., et al. (2007). Saturation of the Terrestrial Carbon Sink. Terrestrial Ecosystems in a Changing World, (Chapter 6), 59–78.

Carlson, T. N., & Ripley, D. A. (1997). On the relation between NDVI, fractional vegetation cover, and leaf area index. *Remote Sensing of Environment*, 62(3), 241–252.

Cernusak, L. A., Hutley, L. B., Beringer, J., Holtum, J. A. M., & Turner, B. L. (2011). Photosynthetic physiology of eucalypts along a sub-continental rainfall gradient in northern Australia. *Agricultural and Forest Meteorology*, 151(11), 1462–1470.

Cleverly, J., Boulain, N., Villalobos-Vega, R., Grant, N., Faux, R., Wood, C., et al. (2013). Dynamics of component carbon fluxes in a semi-arid Acacia woodland, central Australia. *Journal of Geophysical Research: Biogeosciences*, 118(3), 1168–1185.

Dunkerley, D. L. (2002). Infiltration rates and soil moisture in a groved mulga community near Alice Springs, arid central Australia: evidence for complex internal rainwater redistribution in a runoff–runon landscape. *Journal of Arid Environments*, 51(2), 199–219.

Eamus, D., & Cole, S. (1997). Diurnal and Seasonal Comparisons of Assimilation, Phyllode Conductance and Water Potential of Three Acacia and One Eucalyptus Species in the Wet-Dry Tropics of Australia. *Australian Journal of Botany*, 45(2), 275–290.

Eamus, D. (1999). Ecophysiological traits of deciduous and evergreen woody species in the seasonally dry tropics. *Trends in Ecology & Evolution*, 14(1), 11–16.

Eamus, D., Cleverly, J., Boulain, N., Grant, N., Faux, R., & Villalobos-Vega, R. (2013). Carbon and water fluxes in an arid-zone Acacia savanna woodland: An analyses of seasonal patterns and responses to rainfall events. *Agricultural and Forest Meteorology*, 182–183(2013), 225-238.

Eamus, D., Hutley, L. B., & O'Grady, A. P. (2001). Daily and seasonal patterns of carbon and water fluxes above a north Australian savanna. *Tree Physiology*, 21(12-13), 977–988.

Ehleringer, J., & Forseth, I. (1980). Solar Tracking by Plants. *Science*, 210(4474), 1094–1098.

Farquhar, G. D., & Sharkey, T. D. (1982). Stomatal Conductance and Photosynthesis. *Annual Review of Plant Physiology*, 33(1), 317–345.

Fensholt, R., Sandholt, I., & Rasmussen, M. S. (2004). Evaluation of MODIS LAI, fAPAR and the relation between fAPAR and NDVI in a semi-arid environment using in situ measurements. *Remote Sensing of Environment*, 91(3–4), 490–507.

Fisher, R.A., Williams, M., Lola da Costa, A., Malhi, Y., da Costa, R.F., Almeida, S., Meir, P. (2007). The response of an Eastern Amazonian rain forest to drought stress: results and modelling analyses from a throughfall exclusion experiment. *Global Change Biology*. 13, 1-18.

Fordyce, I. R., Duff, G. A., & Eamus, D. (1995). The Ecophysiology of *Allosyncarpia ternata* (Myrtaceae) in Northern Australia: Tree Physiognomy, Leaf Characteristics and Assimilation at Contrasting Sites. *Australian Journal of Botany*, 43(4), 367–377.

Gamon, J. A., Field, C. B., Goulden, M. L., Griffin, K. L., Hartley, A. E., Joel, G., et al. (1995). Relationships between NDVI, canopy structure, and photosynthesis in three Californian vegetation types. *Ecological Applications*, 28–41.

Gitelson, A. A., Peng, Y., Masek, J. G., Rundquist, D. C., Verma, S., Suyker, A., et al. (2012). Remote estimation of crop gross primary production with Landsat data. Remote Sensing of Environment, 121(2012), 404–414.

Gitelson, A. A., Viña, A., Verma, S. B., Rundquist, D. C., Arkebauer, T. J., Keydan, G., et al. (2006). Relationship between gross primary production and chlorophyll content in crops: Implications for the synoptic monitoring of vegetation productivity. *Journal of Geophysical Research*, 111(D8), D08S11.

Gitelson, A. A., Peng, Y., Arkebauer, T. J., & Schepers, J. (2014). Relationships between gross primary production, green LAI, and canopy chlorophyll content in maize: Implications for remote sensing of primary production. *Remote Sensing of Environment*, 144(0), 65–72.

Glenn, E. P., Huete, A. R., Nagler, P. L., & Nelson, S. G. (2008). Relationship between remotely-sensed vegetation indices, canopy attributes and plant physiological processes: What vegetation indices can and cannot tell us about the landscape. *Sensors*, 8(4), 2136–2160.

Goerner, A., Reichstein, M., & Rambal, S. (2009). Tracking seasonal drought effects on ecosystem light use efficiency with satellite-based PRI in a Mediterranean forest. *Remote Sensing of Environment*, 113(5), 1101–1111.

Gower, S. T., Kucharik, C. J., & Norman, J. M. (19959). Direct and Indirect Estimation of Leaf Area Index , fAPAR , and Net Primary Production of Terrestrial Ecosystems. Remote Sensing of Environment, 4257(99), 29–51.

Hanan, N. P., Burba, G., Verma, S. B., Berry, J. A., Suyker, A., & Walter-Shea, E. A. (2002). Inversion of net ecosystem CO2 flux measurements for estimation of canopy PAR absorption. Global Change Biology, 8(6), 563–574.

Heinsch, F. A., Maosheng Zhao, Running, S. W., Kimball, J. S., Nemani, R. R., Davis, K. J., et al. (2006). Evaluation of remote sensing based terrestrial productivity from MODIS using regional tower eddy flux network observations. *IEEE Transactions on Geoscience and Remote Sensing*, 44(7), 1908–1925.

Hoffmann, W. A., da Silva, E. R., Jr, Machado, G. C., Bucci, S. J., Scholz, F. G., Goldstein, G., & Meinzer, F. C. (2005). Seasonal leaf dynamics across a tree density gradient in a Brazilian savanna. *Oecologia*, 145(2), 306–315.

Houborg, R., Anderson, M. C., Daughtry, C. S. T., Kustas, W. P., & Rodell, M. (2010). Using leaf chlorophyll to parameterize light-use-efficiency within a thermal-based carbon, water and energy exchange model. Remote Sensing of Environment, 115(7), 1694–1705.

House, J.I. & Hall, D.O. (2001) Productivity of tropical savannas and grasslands. Terrestrial global productivity: past, present and future (ed. by H. Mooney, J. Roy and B. Saugier), pp. 363–400. Academic Press, San Diego, CA.

Huemmrich, K. F., Privette, J. L., Mukelabai, M., Myneni, R. B., & Knyazikhin, Y. (2005). Time-series validation of MODIS land biophysical products in a Kalahari woodland, Africa. *International Journal of Remote Sensing*, 26(19), 4381–4398.

Huete, A. R., Didan, K., Miura, T., Rodriguez, E. P., Gao, X., & Ferreira, L. G. (2002). Overview of the radiometric and biophysical performance of the MODIS vegetation indices. *Remote Sensing of Environment*, 83(1-2), 195–213.

Huete, A. R., Didan, K., Shimabukuro, Y. E., Ratana, P., Saleska, S. R., Hutyra, L. R., et al. (2006). Amazon rainforests green-up with sunlight in dry season. *Geophysical Research Letters*, 33(6), L06405.

Huete, A. R., Restrepo-Coupe, N., Ratana, P., Didan, K., Saleska, S. R., Ichii, K., et al. (2008). Multiple site tower flux and remote sensing comparisons of tropical forest dynamics in Monsoon Asia. *Agricultural and Forest Meteorology*, 148(5), 748–760.

Hutley, L. B., Grady, A. P. O., & Eamus, D. (2001). Monsoonal influences on evapotranspiration of savanna vegetation of northern Australia. *Oecologia*, 126(3), 434–443.

Jenkins, J. P., Richardson, A. D., Braswell, B. H., Ollinger, S. V., Hollinger, D. Y., & Smith, M. L. (2007). Refining light-use efficiency calculations for a deciduous forest canopy using simultaneous tower-based carbon flux and radiometric measurements. *Agricultural and Forest Meteorology*, 143(1–2), 64–79.

Jiang, Z., Huete, A., Didan, K., & Miura, T. (2008). Development of a two-band enhanced vegetation index without a blue band. *Remote Sensing of Environment*, 112(10), 3833–3845.

Jin, C., Xiao, X., Merbold, L., Arneth, A., Veenendaal, E., & Kutsch, W. L. (2013). Phenology and gross primary production of two dominant savanna woodland ecosystems in Southern Africa. *Remote Sensing of Environment*, 135(0), 189–201.

Jones, D. A., Wang, W., & Fawcett, R. (2009). High-quality spatial climate data-sets for Australia. *Australian Meteorological and Oceanographic Journal*, 58(4), 233–248.

Kanniah, K. D., Beringer, J., Hutley, L. B., Tapper, N. J., & Zhu, X. (2009). Evaluation of Collections 4 and 5 of the MODIS Gross Primary Productivity product and algorithm improvement at a tropical savanna site in northern Australia. *Remote Sensing of Environment*, 113(9), 1808–1822.

Kanniah, K. D., Beringer, J., & Hutley, L. (2010). The comparative role of key environmental factors in determining savanna productivity and carbon fluxes: A review, with special reference to northern Australia. *Progress in Physical Geography*, 34(4), 459–490.

Kanniah, K. D., Beringer, J., & Hutley, L. (2011). Environmental controls on the spatial variability of savanna productivity in the Northern Territory, Australia. *Agricultural and Forest Meteorology*, 151(11), 1429–1439.

Kanniah, K. D., Beringer, J., & Hutley, L. B. (2013). Response of savanna gross primary productivity to interannual variability in rainfall: Results of a remote sensing based light use efficiency model. *Progress in Physical Geography*, 37(6), 1-22.

Kanniah, K. D., Beringer, J., & Hutley, L. (2013). Exploring the link between clouds, radiation, and canopy productivity of tropical savannas. *Agricultural and Forest Meteorology*, 182–183(0), 304–313.

Kasahara, M., Kagawa, T., Oikawa, K., Suetsugu, N., Miyao, M., & Wada, M. (2002). Chloroplast avoidance movement reduces photodamage in plants. *Nature*, 420(6917), 829–832.

Kergoat, L., Lafont, S., Arneth, A., Le Dantec, V., & Saugier, B. (2008). Nitrogen controls plant canopy light-use efficiency in temperate and boreal ecosystems. *Journal of Geophysical Research*, 113(G4), G04017.

Koch, G. W., Vitousek, P. M., Steffen, W. L., & Walker, B. H. (1995). Terrestrial transects for global change research. *Vegetatio*, 121(1-2), 53–65.

Kotchenova, S. Y., & Vermote, E. F. (2007). Validation of a vector version of the 6S radiative transfer code for atmospheric correction of satellite data. Part II. Homogeneous Lambertian and anisotropic surfaces. Applied Optics, 46(20), 4455–4464.

Leuning, R., Cleugh, H. A., Zegelin, S. J., & Hughes, D. (2005). Carbon and water fluxes over a temperate Eucalyptus forest and a tropical wet/dry savanna in Australia: measurements and comparison with MODIS remote sensing estimates. *Agricultural and Forest Meteorology*, 129(3-4), 151–173.

Ludwig, J., Tonway, D., Freudenberger, D., Noble, J., Hodgkinson, K. Eds. (1997). Landscape Ecology, Function and Management: Principles from Australia's Rangelands. CSIRO, Collingwood, Victoria.

Lyapustin, A. (2003). Interpolation and profile correction (IPC) method for shortwave radiative transfer in spectral intervals of gaseous absorption. *Journal of Atmospheric Science*, 60, 865–871.

Ma, X., Huete, A., Yu, Q., Coupe, N. R., Davies, K., Broich, M., et al. (2013). Spatial patterns and temporal dynamics in savanna vegetation phenology across the North Australian Tropical Transect. *Remote Sensing of Environment*, 139(0), 97–115.

Morton, D. C., Nagol, J., Carabajal, C. C., & Rosette, J. (2014). Amazon forests maintain consistent canopy structure and greenness during the dry season. *Nature*, 506(2014), 221-224.

Monteith, J. L. (1972). Solar radiation and productivity in tropical ecosystems. *Journal of Applied Ecology*, 9(3), 747-766.

Monteith, J., & Unsworth, M. (2013). Principles of environmental physics - Plants, Animals, and the Atmosphere. 4th edition. Elsevier, Amsterdam, The Netherlands.

McKeon, G. M., Day, K. A., Howden, S. M., Mott, J. J., Orr, D. M., Scattini, W., & Weston, E. J. (1990). Northern Australian savannas: management for pastoral production. *Journal of Biogeography*, 17(4-5), 355–372.

Myneni, R. B., & Williams, D. L. (1994). On the relationship between FAPAR and NDVI. *Remote Sensing of Environment*, 49(3), 200–211.

NVIS (2007). Australia’s native vegetation - A summary of Australia’s major vegetation groups.

Olofsson, P., Lagergren, F., Lindroth, A., Lindström, J., Klemedtsson, L., Kutsch, W., & Eklundh, L. (2008). Towards operational remote sensing of forest carbon balance across Northern Europe. *Biogeosciences*, 5(3), 817–832.

O'Grady, A. P., Chen, X., Eamus, D., & Hutley, L. B. (2000). Composition, leaf area index and standing biomass of eucalypt open forests near Darwin in the Northern Territory, Australia. *Australian Journal of Botany*, 48(5), 629–638.

O'Grady, A. P., Cook, P. G., Eamus, D., Duguid, A., Wischusen, J. D. H., Fass, T., & Worldege, D. (2009). Convergence of tree water use within an arid-zone woodland. *Oecologia*, 160(4), 643–655.

Ogutu, B. O. (2012). An algorithm to derive the fraction of photosynthetically active radiation absorbed by photosynthetic elements of the canopy (FAPARps) from eddy covariance flux tower data, *New Phytologist*, 197(2), 511-523.

Peng, Y., Gitelson, A. A., Keydan, G., Rundquist, D. C., & Moses, W. (2011). Remote Sensing of Environment. *Remote Sensing of Environment*, 115(4), 978–989.

Peng, Y., Gitelson, A. A., & Sakamoto, T. (2013). Remote estimation of gross primary productivity in crops using MODIS 250m data. *Remote Sensing of Environment*, 128(0), 186–196.

Prior, L. D., Eamus, D., & Duff, G. A. (1997). Seasonal Trends in Carbon Assimilation, Stomatal Conductance, Pre-dawn Leaf Water Potential and Growth in *Terminalia ferdinandiana*, a Deciduous Tree of Northern Australian Savannas. *Australian Journal of Botany*, 45(1), 53–69.

R Core Team (2013). R: A language and environment for statistical computing. Vienna, Austria R Foundation for Statistical Computing.

Rahman, A. F., Sims, D. A., Cordove, V. D., El-Marsri, B. Z. (2005). Potential of MODIS EVI and surface temperature for directly estimating per-pixel ecosystem C fluxes. *Geophysical Research Letters*, 32(19), L19404.

Richardson, A. D., & Hollinger, D. Y. (2005). Statistical modeling of ecosystem respiration using eddy covariance data: maximum likelihood parameter estimation, and Monte Carlo simulation of model and parameter uncertainty, applied to three simple models. *Agricultural and Forest Meteorology*, 131(3), 191–208.

Rossini, M., Migliavacca, M., Galvagno, M., Meroni, M., Cogliati, S., Cremonese, E., et al. (2014). International Journal of Applied Earth Observation and Geoinformation. *International Journal of Applied Earth Observations and Geoinformation*, 29, 1–10.

Ruimy, A., Jarvis, P. G., Baldocchi, D. D., & Saugier, B. (1995). CO_2 Fluxes over Plant Canopies and Solar Radiation: A Review. *Advances in Ecological Research*, 26, 1–68.

Ruimy, A., Kergoat, L., Bondeau, A.(1999). Comparing global models of terrestrial net primary productivity (NPP): analysis of differences in light absorption and light-use efficiency. *Global Change Biology*, 5(S1), 56–64.

Running, S. W., Justice, C. O., & Salomonson, V. (1994). Terrestrial remote sensing science and algorithms planned for EOS/MODIS. International Journal of Remote Sensing. 15(17): 3587-3620.

Running, S. W., Nemani, R. R., Heinsch, F. A., Zhao, M., Reeves, M., & Hashimoto, H. (2004). A continuous satellite-derived measure of global terrestrial primary production. *BioScience*, 54(6), 547–560.

Sims, D. A., Rahman, A. F., Cordova, V. D., Baldocchi, D. D., Flanagan, L. B., Goldstein, A. H., et al. (2005). Midday values of gross CO2 flux and light use efficiency during satellite overpasses can be used to directly estimate eight-day mean flux. *Agricultural and Forest Meteorology*, 131(1-2), 1–12.

Sims, D. A., Rahman, A. F., Cordova, V. D., El-Masri, B. Z., Baldocchi, D. D., Flanagan, L. B., et al. (2006). On the use of MODIS EVI to assess gross primary productivity of North American ecosystems. Journal of Geophysical Research, 111(G4), G04015.

Sims, D. A., Luo, H., Hastings, S., Oechel, W. C., Rahman, A. F., & Gamon, J. A. (2006). Parallel adjustments in vegetation greenness and ecosystem CO2 exchange in response to drought in a Southern California chaparral ecosystem. *Remote Sensing of Environment*, 103(3), 289–303.

Sims, D. A., Rahman, A. F., Cordova, V. D., El-Masri, B. Z., Baldocchi, D. D., Bolstad, P. V., et al. (2008). A new model of gross primary productivity for North American ecosystems based solely on the enhanced vegetation index and land surface temperature from MODIS. *Remote Sensing of Environment*, 112(4), 1633–1646.

Sjöström, M., Ardö, J., Arneth, A., Boulain, N., Cappelaere, B., Eklundh, L., et al. (2011). Exploring the potential of MODIS EVI for modeling gross primary production across African ecosystems. *Remote Sensing of Environment*, 115(4), 1081–1089.

Sjöström, M., Zhao, M., Archibald, S., Arneth, A., Cappelaere, B., Falk, U., et al. (2013). Evaluation of MODIS gross primary productivity for Africa using eddy covariance data. *Remote Sensing of Environment*, 131(0), 275–286.

Thomas, D.S., Eamus, D., 1999. The influence of predawn leaf water potential on stem hydraulic conductivity and foliar ABA concentrations and on stomatal responses to atmospheric water content at constant Ci. *Journal of Experimental Botany.* 50, 243-251.

Thornton, P. E., LAW, B. E., Gholz, H. L., & Clark, K. L. (2002). Modeling and measuring the effects of disturbance history and climate on carbon and water budgets in evergreen needleleaf forests. Agricultural and Forest Meteorology. 113: 185-222.

Turner, D. P., Urbanski, S., Bremer, D., Wofsy, S. C., Meyers, T., Gower, S. T., & Gregory, M. (2003). A cross-biome comparison of daily light use efficiency for gross primary production. *Global Change Biology*, 9(3), 383–395.

Vermote, E. F., Saleous, N. El, Justice, C. O., Kaufman, Y. J., Privette, J. L., Remer, L., et al. (1997). Atmospheric correction of visible to middle-infrared EOS-MODIS data over land surfaces: Background, operational algorithm, and validation. *Journal of Geophysical Research*, 102, 17131–17141.

Vermote, E. F., Saleous, El, N. Z., & Justice, C. O. (2002). Atmospheric correction of MODIS data in the visible to middle infrared: first results. *Remote Sensing of Environment*, 83(1-2), 97-111.

Walker, J., & Gillison, A. N. (1982). Australian savannas. In B. J. Huntley, & B. H. Walker (Eds.), Ecological studies (pp. 5–24). Springer Berlin Heidelberg.

Walker, B. H., Steffen, W. L., Canadell, J., & Ingram, J. S. I. (1999). IGBP Book Series No. 4. The Terrestrial Biosphere and Global Change: Implications for Natural and Managed Ecosystems. Synthesis Volume. Cambridge, UK: Cambridge University Press.

Williams, R. J., Myers, B. A., Muller, W. J., Duff, G. A., & Eamus, D. (1997). Leaf phenology of woody species in a North Australian tropical savanna. *Ecology*, 78(8), 2542–2558.

Whitley, R., Macinnis-NG, C., Hutley, L., Berringer, J., Melanie, Z., Mathew, W., et al. (2011). Is productivity of mesic savannas light limited or water limited? Results of a simulation study. *Global Change Biology*, 17(10), 3130–3149.

Wylie, B. K., Johnson, D. A., Laca, E., Saliendra, N. Z., Gilmanov, T. G., Reed, B. C., et al. (2003). Calibration of remotely sensed, coarse resolution NDVI to CO2 fluxes in a sagebrush–steppe ecosystem. *Remote Sensing of Environment*, 85(2), 243–255.

Woinarski, J., Mackey, B., Nix, H., & Traill, B. (2007). The Nature of Northern Australia. Canberra ACT: ANU E Press.

Wu, C., Niu, Z., Tang, Q., Huang, W., Rivard, B., & Feng, J. (2009). Remote estimation of gross primary production in wheat using chlorophyll-related vegetation indices. *Agricultural and Forest Meteorology*, 149(6-7), 1015–1021.

Wu, C., Niu, Z., & Gao, S. (2010). Gross primary production estimation from MODIS data with vegetation index and photosynthetically active radiation in maize. *Journal of Geophysical Research*, 115(D12), D12127.

Wu, C., Chen, J. M., & Huang, N. (2011). Predicting gross primary production from the enhanced vegetation index and photosynthetically active radiation: Evaluation and calibration. *Remote Sensing of Environment*, 115(12), 3424–3435.

Wu, C., Gonsamo, A., Zhang, F., & Chen, J. M. (2014). ISPRS Journal of Photogrammetry and Remote Sensing. *ISPRS Journal of Photogrammetry and Remote Sensing*, 88(C), 69–79.

Xiao, X., Hollinger, D., Aber, J., Goltz, M., Davidson, E. A., Zhang, Q., & Moore, B., III. (2004). Satellite-based modeling of gross primary production in an evergreen needleleaf forest. *Remote Sensing of Environment*, 89(4), 519–534.

Xiao, X., Zhang, Q., Braswell, B., Urbanski, S., Boles, S., Wofsy, S., et al. (2004). Modeling gross primary production of temperate deciduous broadleaf forest using satellite images and climate data. *Remote Sensing of Environment*, 91(2), 256–270.

Xiao, X., Zhang, Q., Hollinger, D., Aber, J., & Moore, B., III. (2005). Modeling gross primary production of an evergreen needleleaf forest using MODIS and climate data. *Ecological Applications*, 15(3), 954–969.

Yuan, W., Liu, S., Yu, G., Bonnefond, J.-M., Chen, J., Davis, K., et al. (2010). Global estimates of evapotranspiration and gross primary production based on MODIS and global meteorology data. *Remote Sensing of Environment*, 114(7), 1416–1431.

Zhang, Q., Xiao, X., Braswell, B., Linder, E., Baret, F., & Mooreill, B. (2005). Estimating light absorption by chlorophyll, leaf and canopy in a deciduous broadleaf forest using MODIS data and a radiative transfer model. *Remote Sensing of Environment*, 99(3), 357–371.

Zhang, Q., Middleton, E. M., Margolis, H. A., Drolet, G. G., Barr, A. A., & Black, T. A. (n.d.). Can a satellite-derived estimate of the fraction of PAR absorbed by chlorophyll (FAPARchl) improve predictions of light-use efficiency and ecosystem photosynthesis for a boreal aspen forest? *Remote Sensing of Environment*, 113(4), 880–888.

Zhao, M., Heinsch, F. A., Nemani, R. R., & Running, S. W. (2005). Improvements of the MODIS terrestrial gross and net primary production global data set. *Remote Sensing of Environment*, 95(2), 164–176.

Table 1 Summary of EC flux tower sites in the NATT study area.

Site	Longitude (°E)	Latitude (°S)	Elevation (m)	Vegetation Type	Overstorey	Understorey	Canopy Height (m) [a]	Soil [a]	MAP±σ (mm) [b]
Howard Springs	131.150	12.495	64	Eucalypt Woodlands	*Eucalyptus miniata, Erythrophleum chlorostachys, Terminalia ferdinandiana*	*Sorghum spp.*	18.9	red kandosol	1722 ± 341
Adelaide Rivers	131.118	13.077	90	Tropical Eucalypt Woodlands	*E. tectifica, Planchonia careya, Buchanania obovata*	*Sorghum spp.*	12.5	yellow hydrosol	1692 ± 373
Daly River	131.383	14.159	52	Eucalypt Woodlands	*T. grandiflora, E. tetrodonta, E. latifolia*	*Sorghum spp., Heteropogon triticeus*	16.4	red kandosol	1295 ± 334
Ti Tree	133.249	22.283	606	*Acacia* Woodlands	*C. opaca, E. victrix, Acacia aneura*	*Psydrax latifolia, Thyridolepsis michelliana, Eragrostis eriopoda, Eriachne pulchella*	6.5	red kandosol	443 ± 222

[a] cited from OZFlux website: www.ozflux.org.au

[b] MAP = mean annual precipitation, calculated using Australian Bureau of Meteorology gridded rainfall data for each site using data of 12 hydrological years (2000.07.01-2012.06.30) (Jones et al., 2007). To calculate the annual rainfall, we used hydrological year defined from July 1 to following June 30, instead of calendar year.

Table 2 Summary of the coefficients of determination (R^2) between EC tower derived GPP *versus* MOD15A2 LAI/fAPAR, MOD09A1 NDVI/EVI, MOD17A2 GPP and the products of EVI and scaled-LST, tower measured PAR (PAR_{TOC}), and top-of-atmosphere PAR (PAR_{TOA}) at four NATT sites. The highest R^2 for each site or for cross-sites was highlighted in bold.

Predictor	Cross-sites	Howard Springs	Adelaide River	Daly River	Ti Tree
LAI_{MOD15}	0.80	0.59	**0.90**	0.69	0.77
$fAPAR_{MOD15}$	0.72	0.38	0.79	0.63	0.52
GPP_{MOD17}	0.58	0.38	0.69	0.37	0.32
$NDVI_{MOD09}$	0.77	0.58	0.77	0.70	0.47
EVI_{MOD09}	0.84	0.74	0.78	0.78	0.66
$EVI \times LST_{scaled}$	0.81	0.70	0.78	0.69	0.65
$EVI \times PAR_{TOC}$	0.85	0.69	0.86	0.75	0.79
$EVI \times PAR_{TOA}$	**0.87**	**0.78**	0.89	**0.80**	**0.80**

Table 3 Summary of regression coefficients and RMSE between eLUEs and MODIS EVI across four NATT sites, for calibration dataset and validation dataset respectively. The analysis was based on the 8-d temporal resolution time series. The unit of the RMSE is in g C MJ^{-1}. *F* is the F-value, *df* is the degree of freedom, *p* is the p-value.

Dataset	$eLUE_{TOC} = \beta_0 + \beta_1 \times EVI$						
	β_0	β_1	R^2	*F*	df	*p*	RMSE
Calibration	0.0000	1.7771	0.84	902.7	1, 175	< 0.0001	0.0733
Validation	-0.0176	1.8628	0.84	894.3	1, 175	< 0.0001	0.0753
Dataset	$eLUE_{TOA} = \beta_0 + \beta_1 \times EVI$						
	β_0	β_1	R^2	*F*	df	*p*	RMSE
Calibration	0.0303	1.1732	0.81	743	1, 175	< 0.0001	0.0534
Validation	0.0046	1.2731	0.85	1003	1, 175	< 0.0001	0.0500

Table 4 Summary of the regression and error analyses between satellite estimated GPP and EC tower derived GPP across four NATT sites using calibration and validation datasets respectively. The satellite estimated GPP include: MOD17A2 GPP (GPP_{MOD17}), GPP simulated using EVI alone (GPP_{EVI}), GPP simulated by $eLUE_{TOC}$ model (Eq. 20) ($GPP_{eLUE-TOC}$), and GPP simulated using $eLUT_{TOA}$ model (Eq. 21) ($GPP_{eLUE-TOA}$). The analysis was based on the time series of 8-d temporal resolution. The unit of the RMSE is in g C m^{-2} d^{-1}. *F* is the F-value, *df* is the degree of freedom, *p* is the p-value.

Dataset	$GPP_{EC} = \beta_0 + \beta_1 \times GPP_{MOD17}$						
	β_0	β_1	R^2	*F*	df	*p*	RMSE
Calibration	1.2018	0.7454	0.58	240.8	1, 175	< 0.0001	1.4249
Validation	0.9968	0.7863	0.58	240	1, 175	< 0.0001	1.4274
Dataset	$GPP_{EC} = \beta_0 + \beta_1 \times GPP_{EVI}$						
	β_0	β_1	R^2	*F*	Df	*p*	RMSE
Calibration	0.0000	1.0000	0.83	873.6	1, 175	< 0.0001	0.7802
Validation	-0.2636	1.0735	0.85	978.6	1, 175	< 0.0001	0.7766
Dataset	$GPP_{EC} = \beta_0 + \beta_1 \times GPP_{eLUE-TOC}$						
	β_0	β_1	R^2	*F*	df	*p*	RMSE
Calibration	0.1159	0.9593	0.84	924.1	1, 175	< 0.0001	0.7659
Validation	-0.1411	1.0208	0.85	1017	1, 175	< 0.0001	0.7576
Dataset	$GPP_{EC} = \beta_0 + \beta_1 \times GPP_{eLUE-TOA}$						
	β_0	β_1	R^2	*F*	df	*p*	RMSE
Calibration	0.0771	0.9731	0.85	999.9	1, 175	< 0.0001	0.7388
Validation	-0.3198	1.0649	0.88	1297	1, 175	< 0.0001	0.6982

Figure captions

Figure 1 Spatial extent of the NATT study area. The red triangles indicate the locations of the four EC flux tower sites. Background is the Australian Major Vegetation Map (MVGs, v4.1), provided by Australian National Vegetation Information System (NVIS, 2007). Central-right small panel shows the locations of the study area over Australian continent (image source: Google Earth). Photographs show the ground-view of each flux tower site (image source: www.ozflux.org.au). Top-left: early wet season 2010 at Howard Springs; bottom-left: dry season at Daly River; top-right: Adelaide River flux tower; bottom-right: woodland floor and understorey at Ti Tree.

Figure 2 Individual site relationships between satellite indices and EC tower GPP at 8-d time scales. (A) MOD15A2 LAI (LAI_{MOD15}); (B) MOD15A2 fAPAR ($fAPAR_{MOD15}$); (C) MOD17A2 GPP (GPP_{MOD17}); (D) MOD09A1 NDVI ($NDVI_{MOD09}$); (E) MOD09A1 EVI (EVI_{MOD09}). The red dashed line on panel (C) is the 1:1 symmetric line. The blue solid line is the regression line with 95% confidence intervals (grey shaded area).

Figure 3 Cross-sites comparison of satellite indices and EC tower measured GPP across four NATT sites. (A) MOD15A2 LAI (LAI_{MOD15}); (B) MOD15A2 fAPAR ($fAPAR_{MOD15}$); (C) MOD17A2 GPP (GPP_{MOD17}); (D) MOD09A1 NDVI ($NDVI_{MOD09}$); (E) MOD09A1 EVI (EVI_{MOD09}). All $p < 0.0001$. All satellite indices are 8-d temporal resolution. The blue solid line is the regression line with 95% confidence intervals (grey shaded area).

Figure 4 Site-level relationships between EC tower measured GPP and products of EVI with satellite derived or tower measured meteorological variables. The blue solid line is the regression line with 95% confidence intervals (grey shaded area). LST_{scaled} is scaled MODIS daytime land surface temperature (MOD11). PAR_{TOC} and PAR_{TOA} are PAR incident at top-of-canopy and top-of-atmosphere respectively.

Figure 5 Cross-site comparison of scaled temperature and radiation products of EVI and EC tower measured GPP (GPP_{EC}) across four NATT sites. All $p < 0.0001$. All satellite indices are 8-d temporal resolution. The blue solid line is the regression line with 95% confidence intervals (grey shaded area). LST_{scaled} is scaled MODIS daytime land surface temperature (MOD11). PAR_{TOC} and PAR_{TOA} are PAR incident at top-of-canopy and top-of-atmosphere respectively.

Figure 6 Cross-sites relationships between EVI and eLUEs for calibration and validation datasets respectively across four NATT sites. (A) EVI and $eLUE_{TOC}$; (B) EVI and $eLUE_{TOA}$. The blue solid line is the regression line with 95% confidence intervals (grey shaded area). $eLUE_{TOC} = GPP_{EC} / PAR_{TOC}$, and $eLUE_{TOA} = GPP_{EC} / PAR_{TOA}$. PAR_{TOC} and PAR_{TOA} are PAR incident at top-of-canopy and top-of-atmosphere respectively.

Figure 7 Cross-sites relationships between EC tower measured GPP (GPP_{EC}) and MOD17A2 GPP, GPP simulated using EVI alone, and GPP simulated using eLUE models. The blue solid line is the regression line with 95% confidence intervals (grey shaded area). The grey dashed line is the 1:1 symmetric line.

Figure 8 Time series comparison between MOD17A2 GPP (GPP_{MOD17}), GPP simulated using $eLUE_{TOC}$ model ($GPP_{eLUE\text{-}TOC}$, Eq. 20), simulated using $eLUE_{TOA}$ model ($GPP_{eLUE\text{-}TOA}$, Eq. 21), and EC tower measured GPP (GPP_{EC}) across four NATT sites during 2000-2013. All data are at 8-d temporal resolution.

Figure 9 Site-level relationships between satellite estimated GPP and EC tower measured GPP (GPP_{EC}) for green-up and brown-down phases across four NATT sites. (A1-A4) MODIS GPP product (GPP_{MOD17}); (B1-B4) GPP simulated using EVI alone (GPP_{EVI}); (C1-C4) GPP simulated using $eLUE_{TOC}$ model ($GPP_{eLUE\text{-}TOC}$), and (D1-D4) GPP simulated using $eLUE_{TOA}$ model ($GPP_{eLUE\text{-}TOA}$). The green-up phase is defined as the period from left trough before greening season to time when GPP reached a peak, while the brown-down phase is defined as the period following peak GPP to right trough after the cessation of the greening season. The unit of RMSE is g C m^{-2} d^{-1}.

Figure 10 Biogeographic patterns of GPP over the NATT study area during 2000-2013. (1) Mean annual GPP (g C m^{-2} yr^{-1}); (B) coefficient of variance (CV, %) of annual GPP; (C) Mean daily GPP (g C m^{-2} d^{-1}) during the wet season (January-March); (D) mean daily GPP (g C m^{-2} d^{-1}) during the dry season (July-September). The GPP was simulated using the $eLUE_{TOA}$ model driven by PAR_{TOA} (Eq. 21).

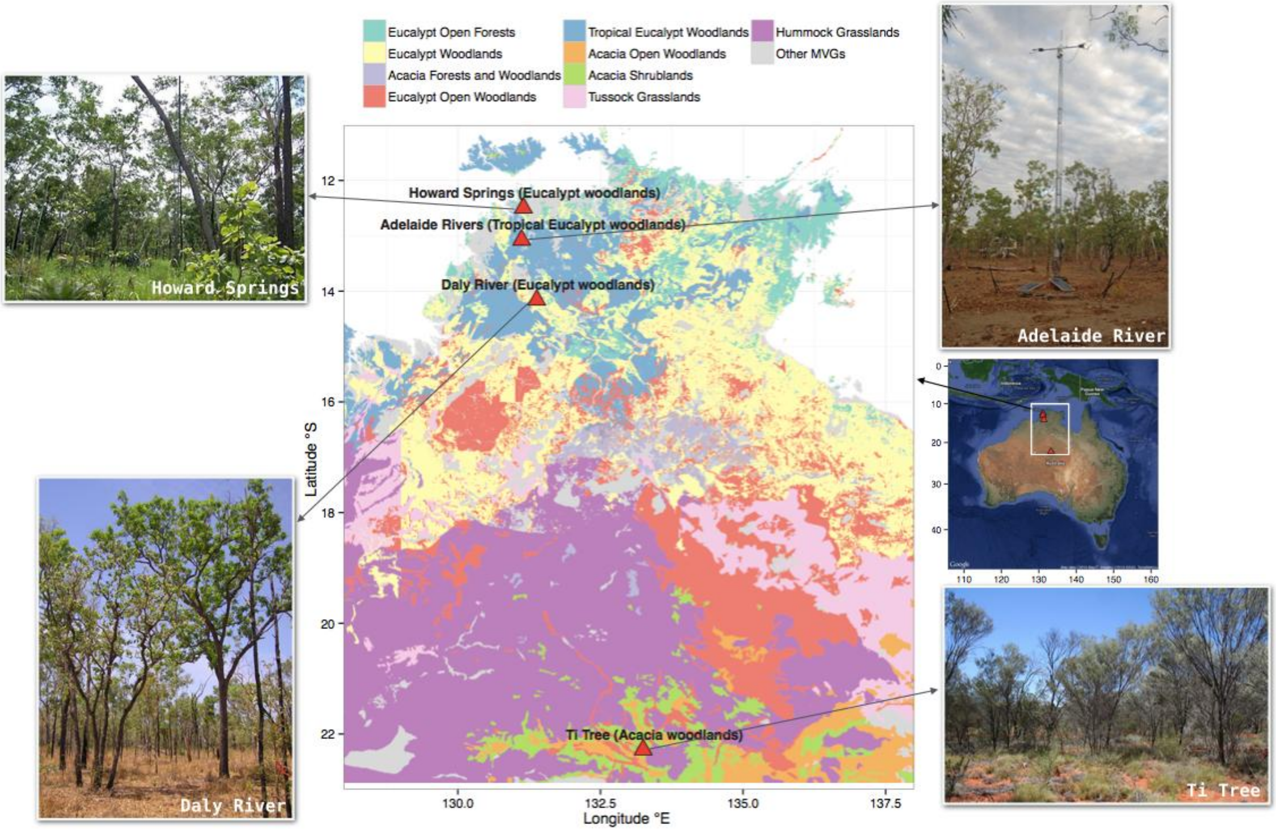

Figure 1 Spatial extent of the NATT study area. The red triangles indicate the locations of the four EC flux tower sites. Background is the Australian Major Vegetation Map (MVGs, v4.1), provided by Australian National Vegetation Information System (NVIS, 2007). Central-right small panel shows the locations of the study area over Australian continent (image source: Google Earth). Photographs show the ground-view of each flux tower site (image source: www.ozflux.org.au). Top-left: early wet season 2010 at Howard Springs; bottom-left: dry season at Daly River; top-right: Adelaide River flux tower; bottom-right: woodland floor and understorey at Ti Tree.

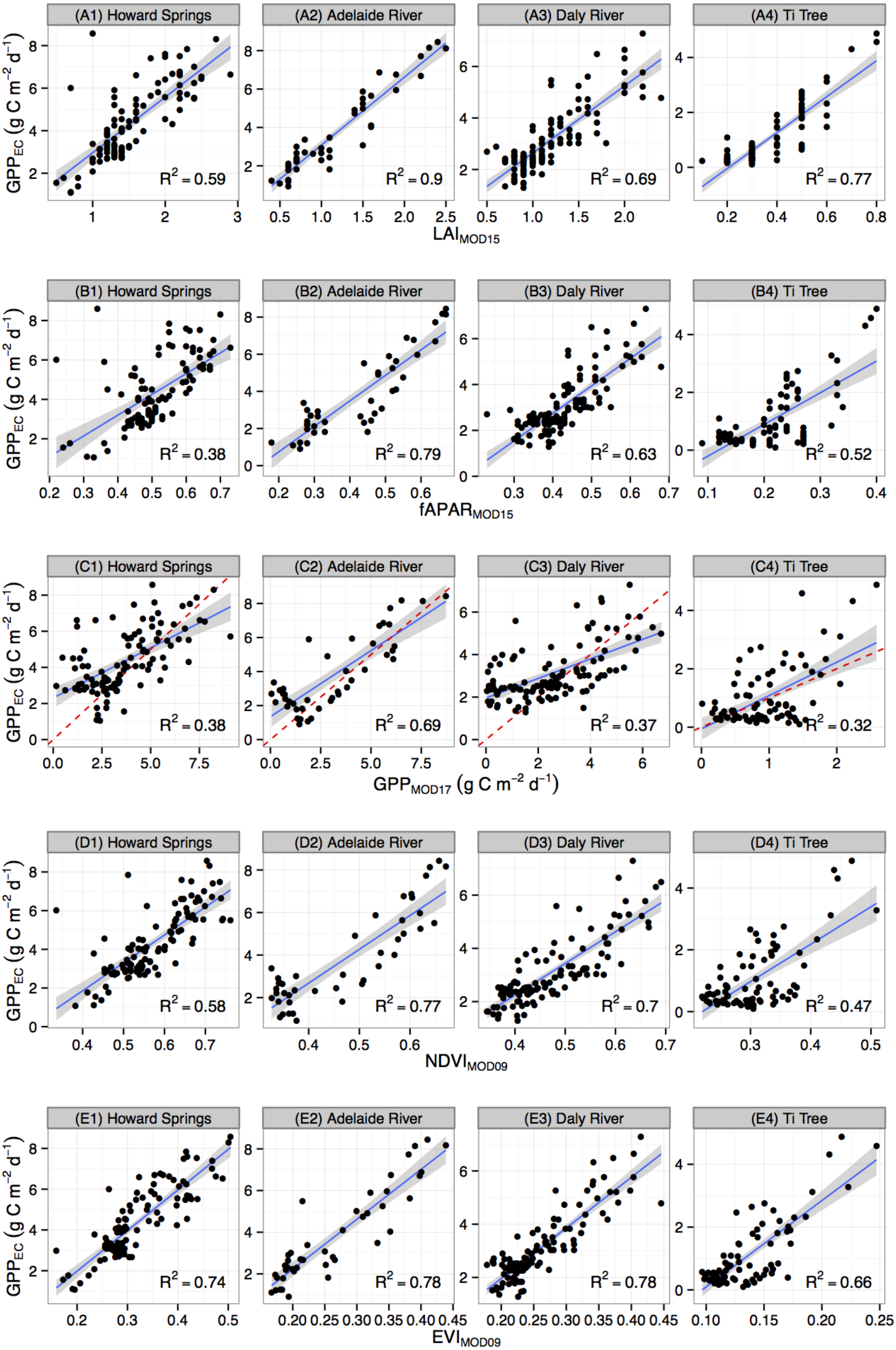
(A1) Howard Springs
(A2) Adelaide River
(A3) Daly River
(A4) Ti Tree
$R^2 = 0.59$
$R^2 = 0.9$
$R^2 = 0.69$
$R^2 = 0.77$
LAI_{MOD15}
(B1) Howard Springs
(B2) Adelaide River
(B3) Daly River
(B4) Ti Tree
$R^2 = 0.38$
$R^2 = 0.79$
$R^2 = 0.63$
$R^2 = 0.52$
$fAPAR_{MOD15}$
(C1) Howard Springs
(C2) Adelaide River
(C3) Daly River
(C4) Ti Tree
$R^2 = 0.38$
$R^2 = 0.69$
$R^2 = 0.37$
$R^2 = 0.32$
GPP_{MOD17} (g C m^{-2} d^{-1})
(D1) Howard Springs
(D2) Adelaide River
(D3) Daly River
(D4) Ti Tree
$R^2 = 0.58$
$R^2 = 0.77$
$R^2 = 0.7$
$R^2 = 0.47$
$NDVI_{MOD09}$
(E1) Howard Springs
(E2) Adelaide River
(E3) Daly River
(E4) Ti Tree
$R^2 = 0.74$
$R^2 = 0.78$
$R^2 = 0.78$
$R^2 = 0.66$
EVI_{MOD09}
GPP_{EC} (g C m^{-2} d^{-1})

Figure 2 Individual site relationships between satellite indices and EC tower GPP at 8-d time scales. (A) MOD15A2 LAI (LAI_{MOD15}); (B) MOD15A2 fAPAR ($fAPAR_{MOD15}$); (C) MOD17A2 GPP (GPP_{MOD17}); (D) MOD09A1 NDVI ($NDVI_{MOD09}$); (E) MOD09A1 EVI (EVI_{MOD09}). The red dashed line on panel (C) is the 1:1 symmetric line. The blue solid line is the regression line with 95% confidence intervals (grey shaded area).

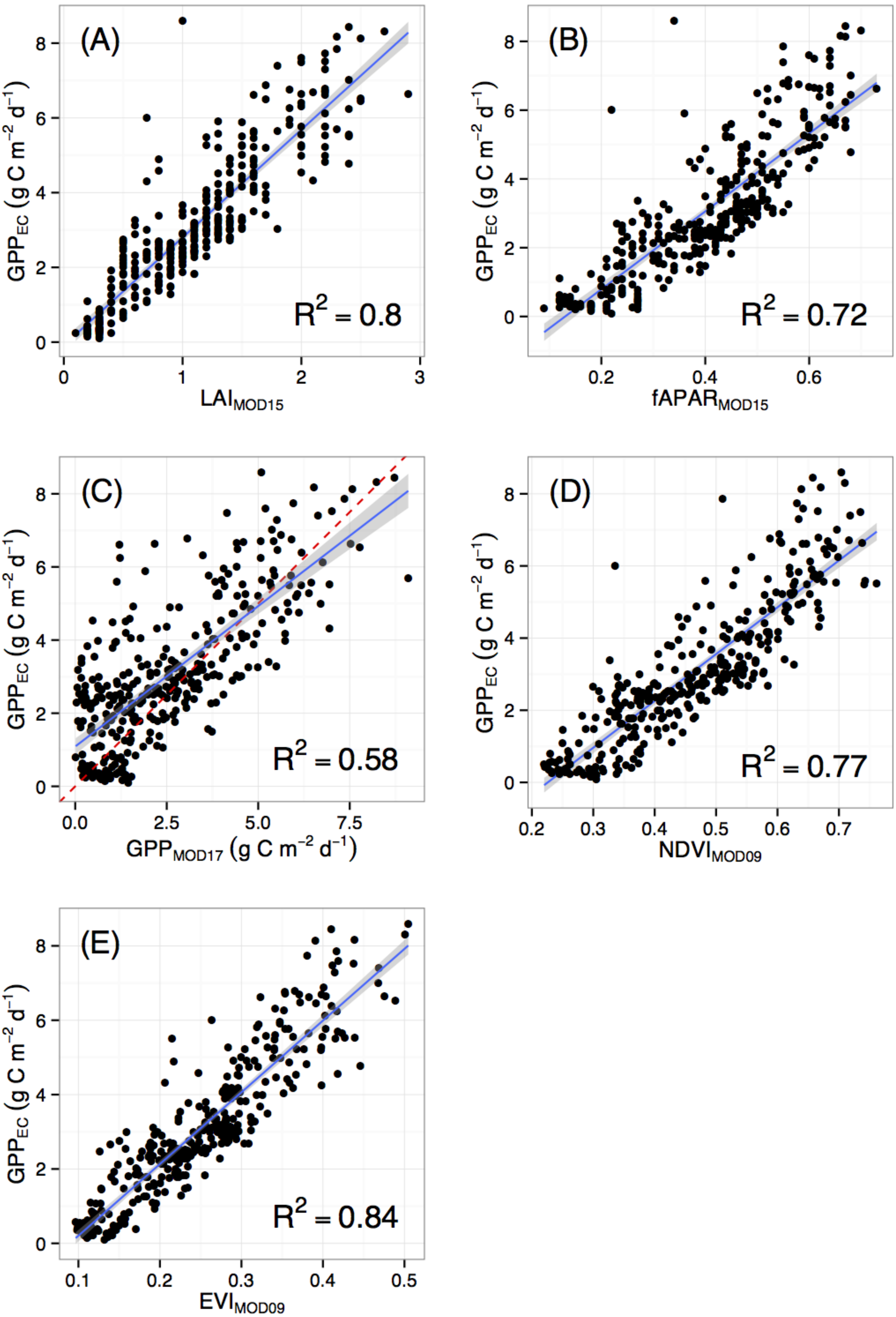
(A)
R2 = 0.8
GPPEC (g C m−2 d−1)
LAIMOD15
(B)
R2 = 0.72
GPPEC (g C m−2 d−1)
fAPARMOD15
(C)
R2 = 0.58
GPPEC (g C m−2 d−1)
GPPMOD17 (g C m−2 d−1)
(D)
R2 = 0.77
GPPEC (g C m−2 d−1)
NDVIMOD09
(E)
R2 = 0.84
GPPEC (g C m−2 d−1)
EVIMOD09

Figure 3 Cross-sites comparison of satellite indices and EC tower measured GPP across four NATT sites. (A) MOD15A2 LAI (LAI_{MOD15}); (B) MOD15A2 fAPAR ($fAPAR_{MOD15}$); (C) MOD17A2 GPP (GPP_{MOD17}); (D) MOD09A1 NDVI ($NDVI_{MOD09}$); (E) MOD09A1 EVI (EVI_{MOD09}). All $p < 0.0001$. All satellite indices are 8-d temporal resolution. The blue solid line is the regression line with 95% confidence intervals (grey shaded area).

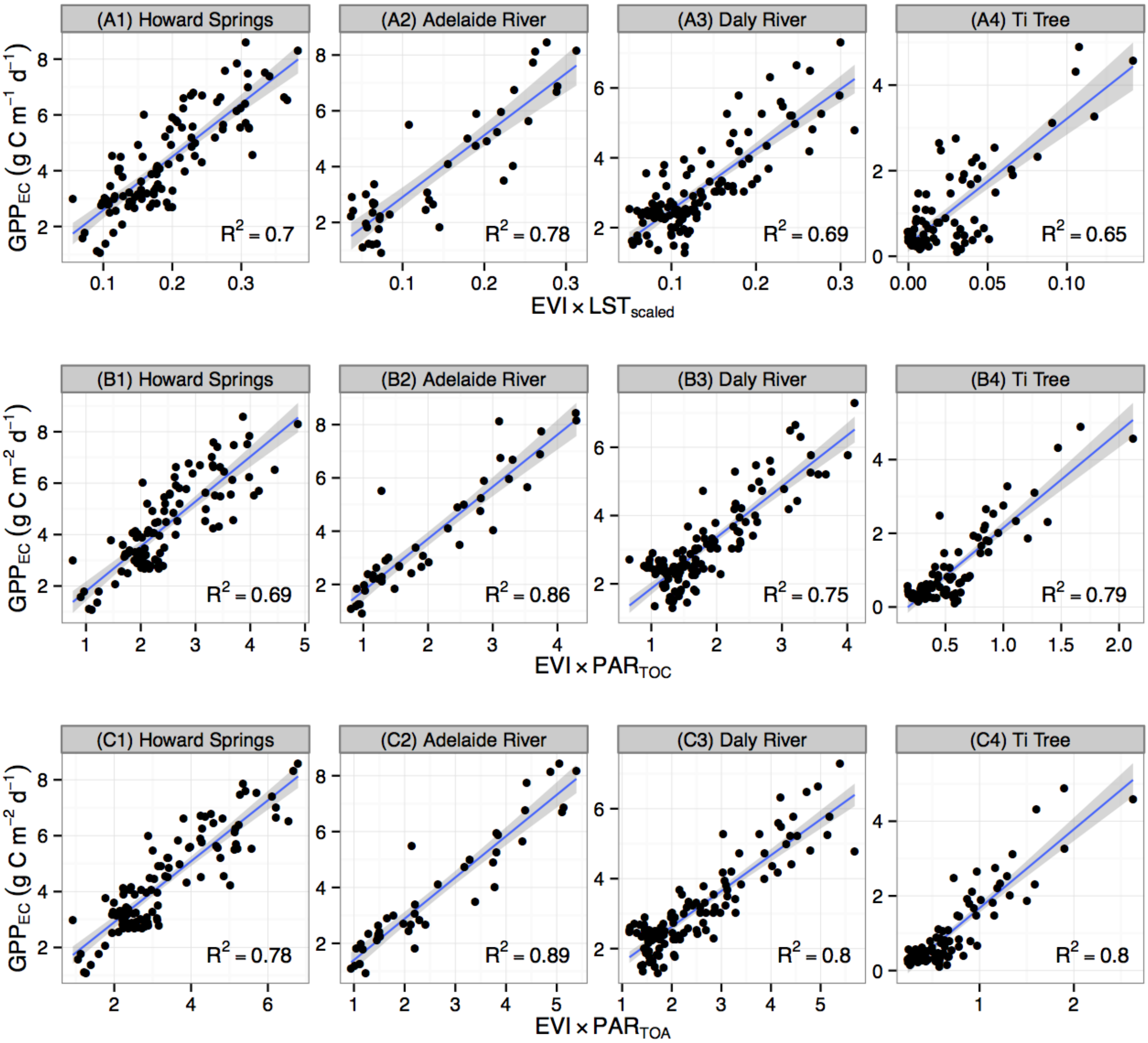

Figure 4 Site-level relationships between EC tower measured GPP and products of EVI with satellite derived or tower measured meteorological variables. The blue solid line is the regression line with 95% confidence intervals (grey shaded area). LST_{scaled} is scaled MODIS daytime land surface temperature (MOD11). PAR_{TOC} and PAR_{TOA} are PAR incident at top-of-canopy and top-of-atmosphere respectively.

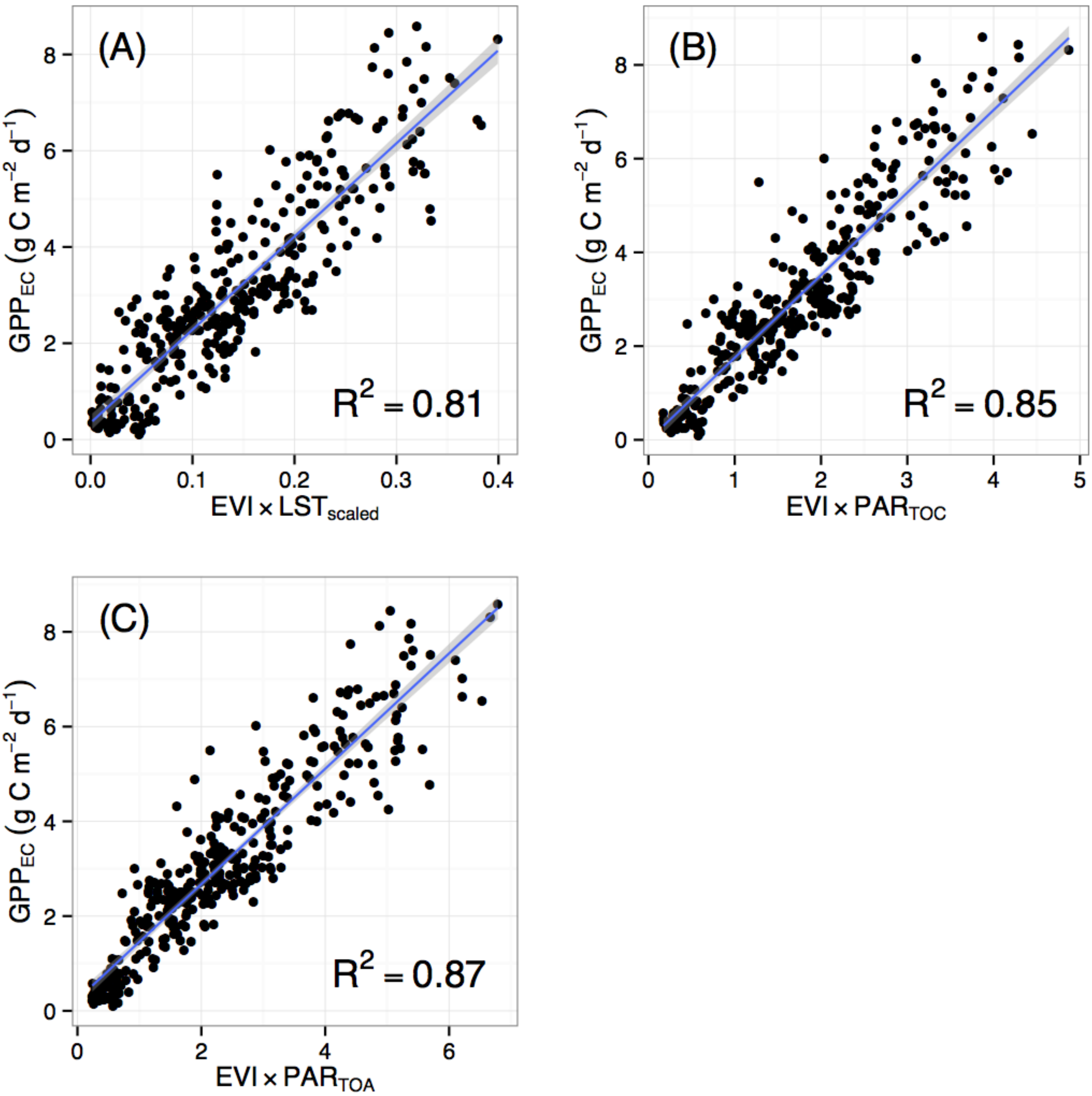

Figure 5 Cross-site comparison of scaled temperature and radiation products of EVI and EC tower measured GPP (GPP_{EC}) across four NATT sites. All $p < 0.0001$. All satellite indices are 8-d temporal resolution. The blue solid line is the regression line with 95% confidence intervals (grey shaded area). LST_{scaled} is scaled MODIS daytime land surface temperature (MOD11). PAR_{TOC} and PAR_{TOA} are PAR incident at top-of-canopy and top-of-atmosphere respectively.

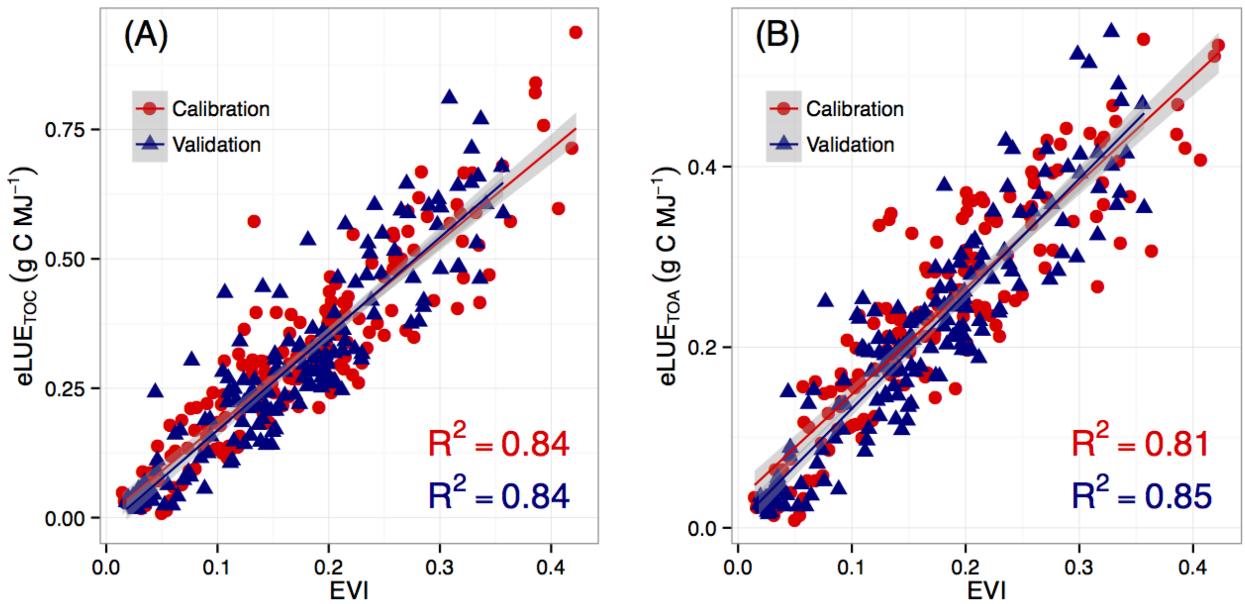

Figure 6 Cross-sites relationships between EVI and eLUEs for calibration and validation datasets respectively across four NATT sites. (A) EVI and eLUE$_{TOC}$; (B) EVI and eLUE$_{TOA}$. The blue solid line is the regression line with 95% confidence intervals (grey shaded area). eLUE$_{TOC}$ = GPP$_{EC}$ / PAR$_{TOC}$, and eLUE$_{TOA}$ = GPP$_{EC}$ / PAR$_{TOA}$. PAR$_{TOC}$ and PAR$_{TOA}$ are PAR incident at top-of-canopy and top-of-atmosphere respectively.

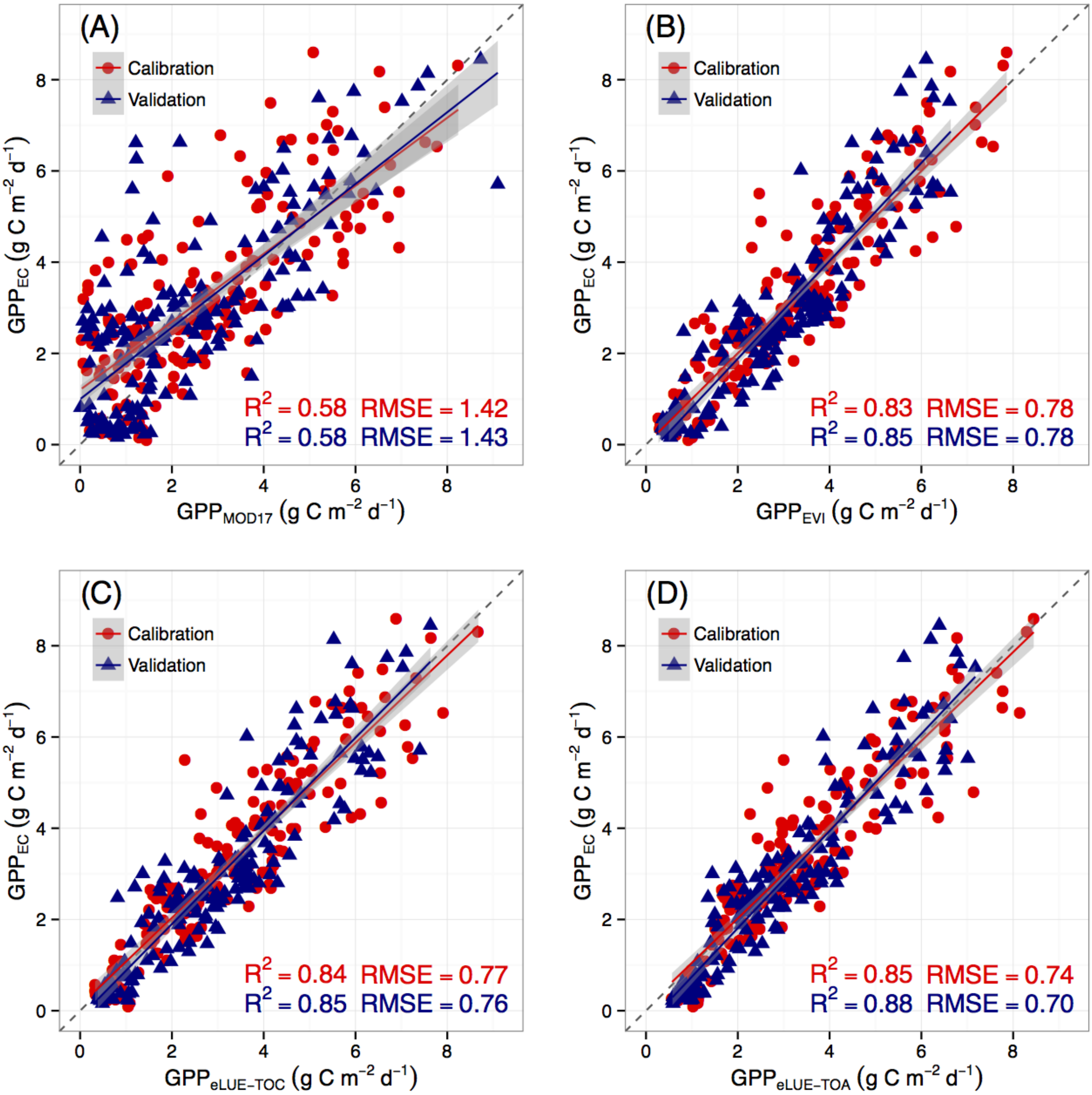

Figure 7 Cross-sites relationships between EC tower measured GPP (GPP_{EC}) and MOD17A2 GPP (GPP_{MOD17}), GPP simulated using EVI alone (GPP_{EVI}), and GPP simulated using eLUE models ($GPP_{eLUE-TOC}$ and $GPP_{eLUE-TOA}$). The blue solid line is the regression line with 95% confidence intervals (grey shaded area). The grey dashed line is the 1:1 symmetric line.

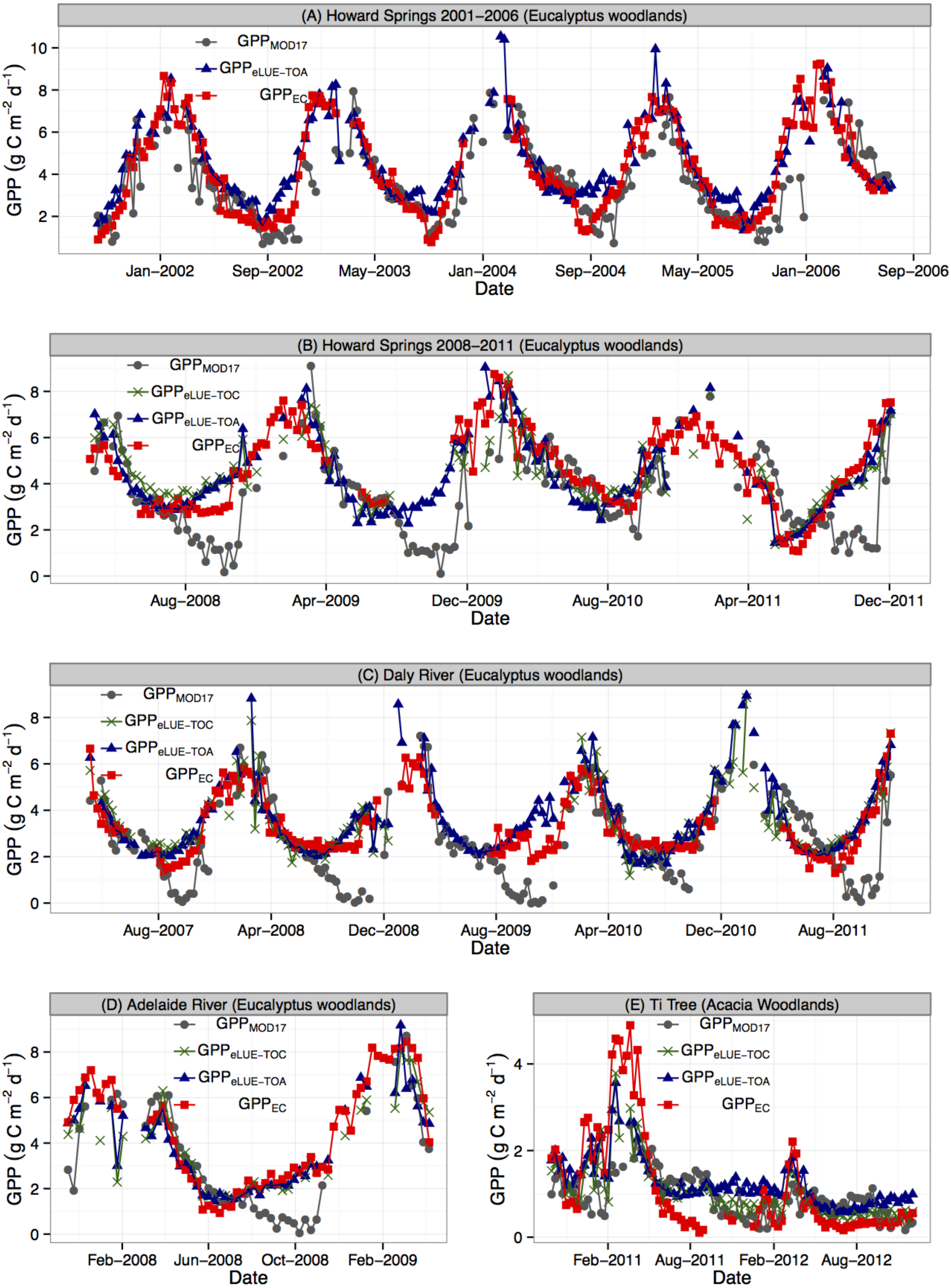

Figure 8 Time series comparison between MOD17A2 GPP (GPP_{MOD17}), GPP simulated using $eLUE_{TOC}$ model ($GPP_{eLUE\text{-}TOC}$, Eq. 20), simulated using $eLUE_{TOA}$ model ($GPP_{eLUE\text{-}TOA}$, Eq. 21), and

EC tower measured GPP (GPP_{EC}) across four NATT sites during 2000-2013. All data are at 8-d temporal resolution.

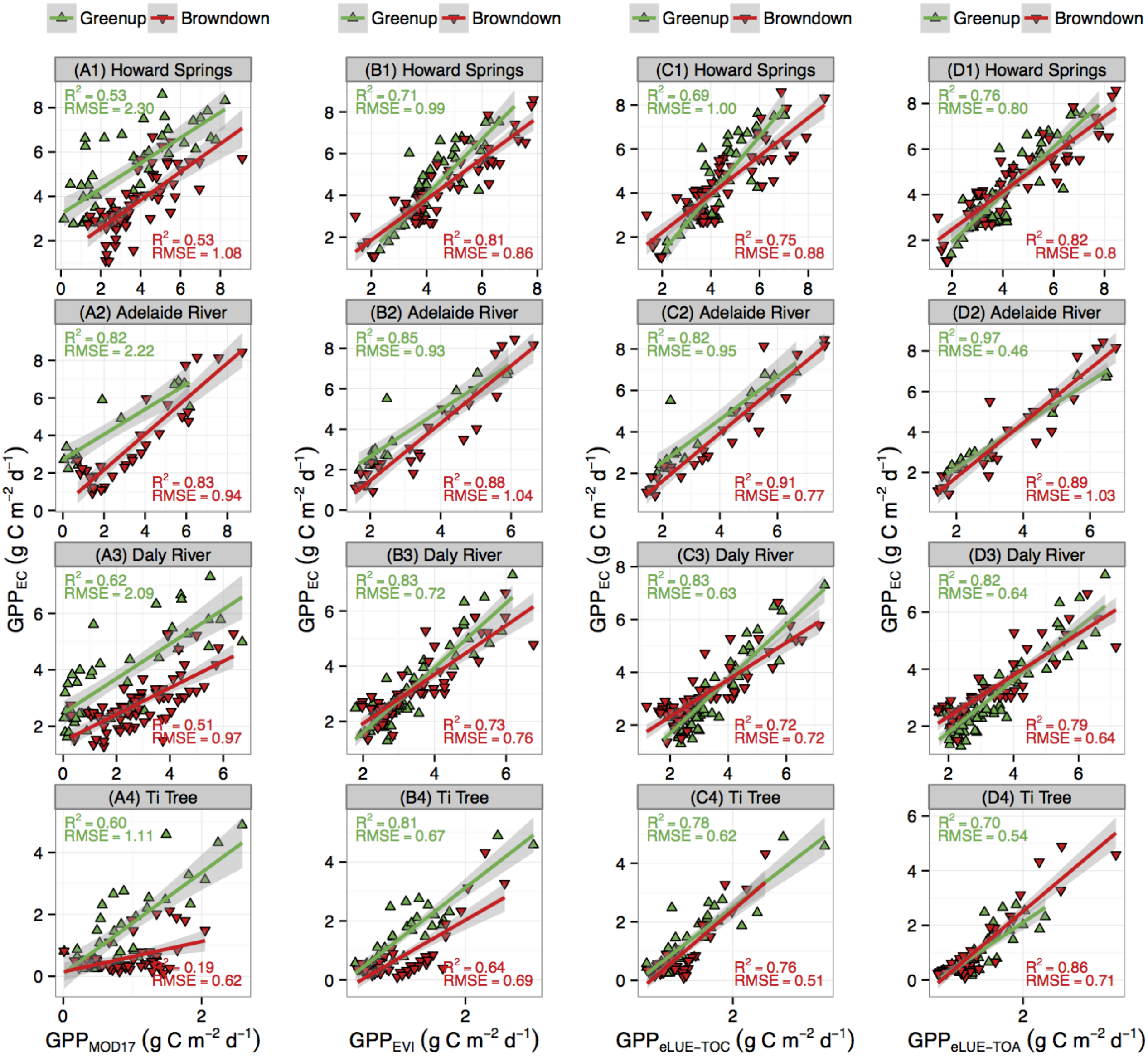

Figure 9 Site-level relationships between satellite estimated GPP and EC tower measured GPP (GPP_{EC}) for green-up and brown-down phases across four NATT sites. (A1-A4) MODIS GPP product (GPP_{MOD17}); (B1-B4) GPP simulated using EVI alone (GPP_{EVI}); (C1-C4) GPP simulated using $eLUE_{TOC}$ model ($GPP_{eLUE\text{-}TOC}$), and (D1-D4) GPP simulated using $eLUE_{TOA}$ model ($GPP_{eLUE\text{-}TOA}$). The green-up phase is defined as the period from left trough before greening season to time when GPP reached a peak, while the brown-down phase is defined as the period following peak GPP to right trough after the cessation of the greening season. The unit of RMSE is g C m^{-2} d^{-1}.

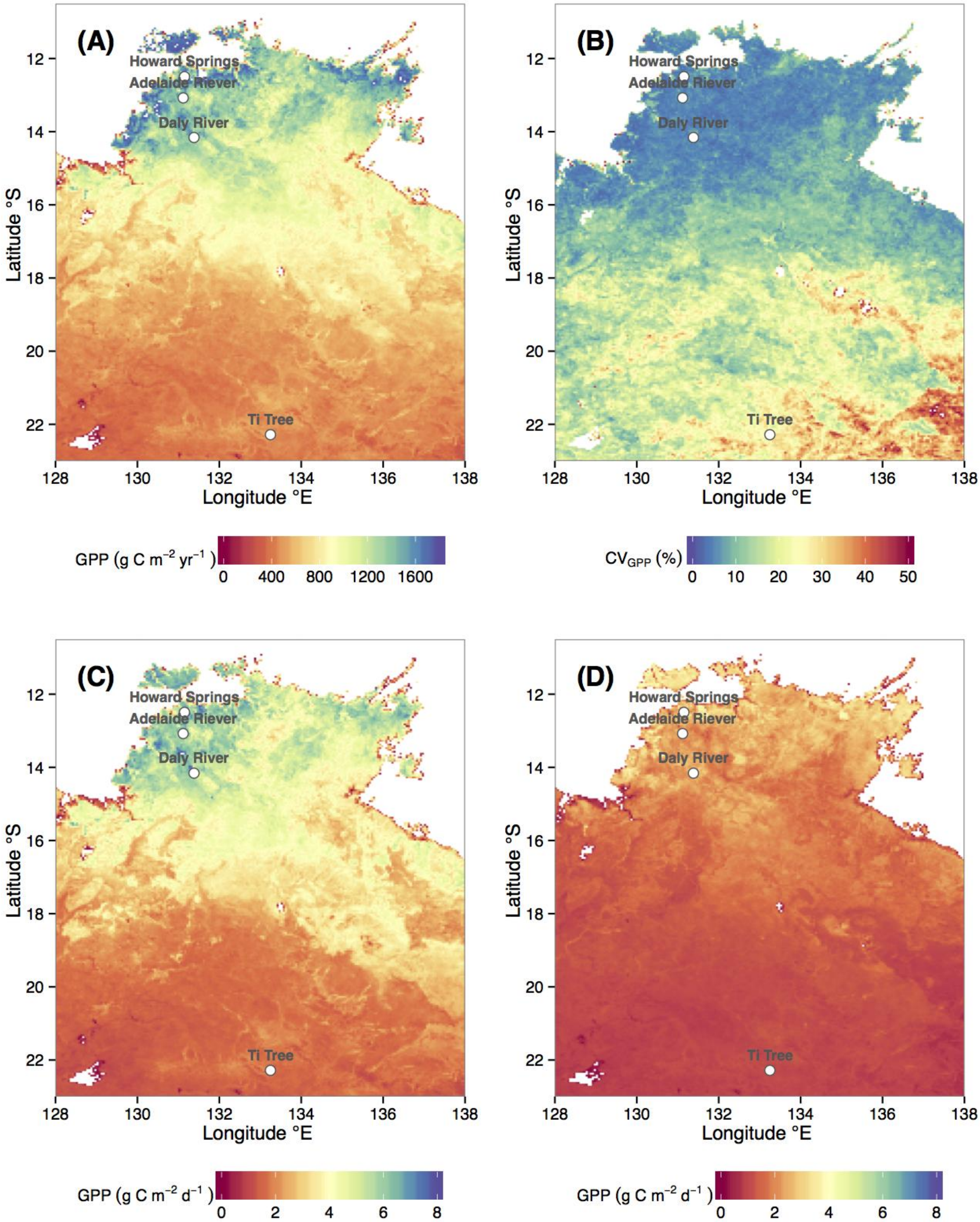

Figure 10 Biogeographic patterns of GPP over the NATT study area during 2000-2013. (1) Mean annual GPP (g C m^{-2} yr^{-1}); (B) coefficient of variance (CV, %) of annual GPP; (C) Mean daily GPP (g C m^{-2} d^{-1}) during the wet season (January-March); (D) mean daily GPP (g C m^{-2} d^{-1}) during the

dry season (July-September). The GPP was simulated using the $eLUE_{TOA}$ model driven by PAR_{TOA} (Eq. 21).

KML File (for GoogleMaps)

Click here to download KML File (for GoogleMaps): NATT.kml